



Deposited via The University of Leeds.

White Rose Research Online URL for this paper:

<https://eprints.whiterose.ac.uk/id/eprint/128273/>

Version: Accepted Version

---

**Article:**

Bate, N, Caves, RE, Skinner, SP et al. (2018) A Novel Mechanism for Calmodulin Dependent Inactivation of Transient Receptor Potential Vanilloid 6. *Biochemistry*, 57 (18). pp. 2611-2622. ISSN: 0006-2960

<https://doi.org/10.1021/acs.biochem.7b01286>

---

**Reuse**

Items deposited in White Rose Research Online are protected by copyright, with all rights reserved unless indicated otherwise. They may be downloaded and/or printed for private study, or other acts as permitted by national copyright laws. The publisher or other rights holders may allow further reproduction and re-use of the full text version. This is indicated by the licence information on the White Rose Research Online record for the item.

**Takedown**

If you consider content in White Rose Research Online to be in breach of UK law, please notify us by emailing [eprints@whiterose.ac.uk](mailto:eprints@whiterose.ac.uk) including the URL of the record and the reason for the withdrawal request.

## A Novel Mechanism for Calmodulin Dependent Inactivation of Transient Receptor Potential Vanilloid 6

Neil Bate, Rachel E. Caves, Simon P. Skinner, Ben T. Goult,  
Jaswir Basran, John S. Mitcheson, and Geerten W. Vuister

*Biochemistry*, **Just Accepted Manuscript** • DOI: 10.1021/acs.biochem.7b01286 • Publication Date (Web): 05 Mar 2018

Downloaded from <http://pubs.acs.org> on March 6, 2018

### Just Accepted

“Just Accepted” manuscripts have been peer-reviewed and accepted for publication. They are posted online prior to technical editing, formatting for publication and author proofing. The American Chemical Society provides “Just Accepted” as a service to the research community to expedite the dissemination of scientific material as soon as possible after acceptance. “Just Accepted” manuscripts appear in full in PDF format accompanied by an HTML abstract. “Just Accepted” manuscripts have been fully peer reviewed, but should not be considered the official version of record. They are citable by the Digital Object Identifier (DOI®). “Just Accepted” is an optional service offered to authors. Therefore, the “Just Accepted” Web site may not include all articles that will be published in the journal. After a manuscript is technically edited and formatted, it will be removed from the “Just Accepted” Web site and published as an ASAP article. Note that technical editing may introduce minor changes to the manuscript text and/or graphics which could affect content, and all legal disclaimers and ethical guidelines that apply to the journal pertain. ACS cannot be held responsible for errors or consequences arising from the use of information contained in these “Just Accepted” manuscripts.



1  
2  
3  
4  
5  
6 **A Novel Mechanism for Calmodulin Dependent Inactivation of Transient**  
7 **Receptor Potential Vanilloid 6**  
8  
9

10  
11  
12 Neil Bate, Rachel E. Caves<sup>‡</sup>, Simon P. Skinner<sup>†</sup>, Benjamin T. Goult<sup>#</sup>, Jaswir Basran,  
13 John S. Mitcheson & Geerten W. Vuister<sup>\*</sup>  
14  
15

16  
17  
18  
19 Department of Molecular and Cell Biology, Leicester Institute of Structural and  
20 Chemical Biology, University of Leicester  
21 Henry Wellcome Building, Lancaster Road, Leicester, LE1 9HN, United Kingdom.  
22  
23

24  
25  
26  
27 <sup>‡</sup>Present address:

28  
29 School of Physiology, Pharmacology and Neuroscience. Faculty of Biomedical  
30 Sciences, University of Bristol, University Walk, Bristol, BS8 1TD  
31 United Kingdom.  
32  
33

34  
35 <sup>†</sup>Present address:

36  
37 School of Molecular and Cellular Biology, Faculty of Biological Sciences & Astbury  
38 Centre for Structural Molecular Biology, University of Leeds, Leeds, LS2 9JT, United  
39 Kingdom.  
40  
41

42  
43 <sup>#</sup>Present address:

44  
45 School of Biosciences, University of Kent, Canterbury, Kent, CT2 7NJ, United  
46 Kingdom.  
47  
48

49  
50  
51 <sup>\*</sup>Corresponding author (gv29@leicester.ac.uk)  
52  
53

54  
55 running title: Calmodulin Dependent Inactivation of TRPV6  
56  
57

**Abstract**

The paralogues TRPV5 and TRPV6 belong to the vanilloid subfamily of the Transient Receptor Potential (TRP) superfamily of ion channels and both play an important role in overall  $\text{Ca}^{2+}$  homeostasis. The functioning of the channels centres on a tightly controlled  $\text{Ca}^{2+}$ -dependent feedback mechanism where the direct binding of the universal  $\text{Ca}^{2+}$ -binding protein calmodulin (CaM) to the channel's C-terminal tail is required for channel inactivation. We have investigated this interaction at the atomic level and propose that under basal cellular  $[\text{Ca}^{2+}]$  CaM is constitutively bound to the channel's C-tail via CaM C-lobe only contacts. When cytosolic  $[\text{Ca}^{2+}]$  increases charging the apo CaM N-lobe with  $\text{Ca}^{2+}$ , the CaM:TRPV6 complex rearranges and the TRPV6 C-tail further engages the CaM N-lobe via a crucial interaction involving L707. In a cellular context, mutation of L707 significantly increased the rate of channel inactivation. Finally, we present a model for TRPV6 CaM-dependent inactivation, which involves a novel so-called "two-tail" mechanism whereby CaM bridges between two TRPV6 monomers resulting in closure of the channel pore.

**keywords**

TRPV6 calcium channel ; NMR ; ITC ; electrophysiology ; Calmodulin

## Introduction

In humans, the Transient Receptor Potential (TRP)<sup>‡</sup> superfamily of twenty-seven ion channels are divided into six sub-groups (TRPC; TRPV; TRPM; TRPP; TRPA; TRPML). The members of the TRP superfamily have been grouped together based on proposed structural homology, such that members within each group are functionally diverse and expressed in a wide array of cell and tissue types<sup>1</sup>. Fundamental physiological roles have been clearly established from the identification of channel dysfunction-related pathologies (channelopathies)<sup>2</sup>, in addition to aberrant gene expression studies in various cancer cell types<sup>3</sup>. Recently, the structures of the transmembrane spanning parts of four distinct TRP channels have been solved; TRPV1<sup>4</sup>, TRPV2<sup>5</sup>, TRPV5<sup>6</sup> and TRPA1<sup>7</sup> by cryo-EM whereas TRPV6 has been solved by both X-ray crystallography<sup>8</sup> and by cryo-EM<sup>9</sup>. These analyses confirmed the previously postulated channel topology; i.e. native channels are tetrameric with each TRP subunit consisting of six transmembrane helices. Helices five and six of each subunit are arranged within the tetramer to form the ion-conducting pore, analogous to potassium channels and an iris-like channel opening. Each transmembrane region is flanked by cytosolic N- and C-termini of varying lengths<sup>10</sup>. Moreover, the C-termini are in close proximity to the pore and surrounded by an outer skirt consisting of the N-terminal ankyrin repeats.

The epithelial Ca<sup>2+</sup> channel TRPV6 is a member of the vanilloid subfamily and, together with its paralogue TRPV5, perform an important role in Ca<sup>2+</sup> homeostasis<sup>11</sup>. These channels are highly selective for Ca<sup>2+</sup><sup>12,13</sup> and are expressed within a range of epithelial cell types<sup>12,14</sup>. Unlike *Trpv5*<sup>-/-</sup> null-mice, which exhibited a defect in bone formation due to excessive loss of Ca<sup>2+</sup> in the urine<sup>15</sup>, *Trpv6*<sup>-/-</sup> null-mice were still viable on a normal calcium diet<sup>16</sup>; however they exhibited an increase in male sterility due to a block in Ca<sup>2+</sup> uptake by the epididymal epithelium<sup>16</sup>.

In order to tightly regulate Ca<sup>2+</sup> entry into the cell, TRP channels engage a Ca<sup>2+</sup>-dependent feedback mechanism(s) to inactivate the channel (channel gating).

---

<sup>‡</sup> **Abbreviations** CaM: Calmodulin; C-tail: C-terminal tail of the TRPV6 channel; CSP: chemical shift perturbation; EM: Electron Microscopy; FRET: Foster resonance energy transfer; ITC: isothermal titration calorimetry; NMR: nuclear magnetic resonance; N-tail: N-terminal tail of the TRPV6 channel; TRP: transient receptor potential; TRPV: transient receptor potential vanilloid; HEK293: human embryonic kidney; GB1: B1 domain of protein G.

1  
2  
3 Thus, on the basis of experiments in whole HEK293 cells TRPV6 channel  
4 inactivation was proposed to occur via a fast  $\text{Ca}^{2+}$ -dependent component together with  
5 a slower CaM-dependent component<sup>17,18</sup>. A number of  $\text{Ca}^{2+}$ -responsive proteins have  
6 been shown to directly interact with TRPV5 and/or TRPV6; these include Calbindin-  
7  $\text{D}_{28\text{K}}$ <sup>19</sup>, 80-KH<sup>20</sup> and Calmodulin (CaM)<sup>21-24</sup>. Peptide scanning using *in silico*  
8 predicted CaM binding sites identified five short TRPV5 peptide sequences capable  
9 of binding CaM<sup>23-25</sup>. Moreover, deletion of the C-terminal TRPV5 CaM binding site  
10 <sup>26</sup> or mutation of the analogous region in TRPV6<sup>18</sup> significantly increases cellular  
11  $[\text{Ca}^{2+}]$  without altering the membrane localisation of the channels in HEK293 cells.  
12 These observations for TRPV5 and TRPV6 are in line with those observed for other  
13 TRP channels; for example, channel desensitisation has also been achieved by  
14 deletion of the membrane distal C-terminal CaM binding site in either TRPC1<sup>27</sup>,  
15 TRPV1<sup>28</sup> or TRPV4<sup>29</sup>. In addition, CaM has also been shown to bind to the  
16 cytosolic C-tails of TRPV2<sup>30</sup>, strongly suggesting a similar mode of CaM-dependent  
17 channel inactivation within the TRPV family.

18  
19 Taken together, these analyses strongly implicate the binding of CaM to the  
20 TRP C-tail as a key event in channel inactivation. CaM is a well-known ion channel  
21 regulator and has been proven to be very adaptable in its interaction with different  
22 targets<sup>31,32</sup>. CaM consists of two independent globular domains, denoted as the N-lobe  
23 and the C-lobe, linked by a flexible region (Fig. S1A). Each lobe independently binds  
24 two  $\text{Ca}^{2+}$  ions; although *in vitro*, the C-lobe has a 6-fold higher affinity for free  $\text{Ca}^{2+}$   
25 than the N-lobe<sup>33</sup>.

26  
27 To the best of our knowledge, a viable molecular mechanism for TRP channel  
28 inactivation by CaM has thus far remained elusive. Moreover, neither the EM nor the  
29 X-ray TRP channel structures provide any clues, as the relevant C-tails are missing in  
30 all of these structures either as a result of truncations used for performing the  
31 structural studies or due to the disordered nature of the N- and C-termini. Therefore,  
32 for the first time we present an experimentally-derived model which details how, in a  
33 cellular context, TRPV6 can be inactivated by CaM in response to elevated  $[\text{Ca}^{2+}]$  via  
34 a novel so-called “two-tail mechanism”. Using a combined approach involving NMR  
35 spectroscopy, ITC and analytical gel filtration together with electrophysiology, we  
36 present data that show the CaM-dependent TRPV6 inactivation process to comprise  
37 of three distinct states of the CaM:channel complex. In the accompanying paper by  
38 Bokhovchuk et al.<sup>52</sup>, we report on a structural and dynamical analysis of the complex

1  
2  
3 of CaM with the TRPV5 paralogue representing the channel under basal Ca<sup>2+</sup>  
4 conditions. We identify key residues for the inactivation process, including L707A, a  
5 point mutation that sensitises the system, causing an increased rate of channel  
6 inactivation in response to increased cellular [Ca<sup>2+</sup>]. We rationalise that the  
7 mechanism proposed here is potentially also applicable to other CaM-dependent  
8 inactivated TRP channels.  
9  
10  
11  
12

## 13 **Materials and Methods**

### 14 **Plasmids**

15  
16 The TRPV6<sup>655-722</sup> region and mutants thereof, were generated by PCR and cloned into  
17 the *E. coli* protein expression vector pLEICS-46, which contains a N-terminal GB1  
18 solubility tag, a His<sub>6</sub> affinity tag followed by a TEV cleavage site (Protex, Leicester  
19 University). CaM wild-type and mutants thereof, were generated by PCR and inserted  
20 into the *E. coli* protein expression vector pLEICS-01, which contains a His<sub>6</sub> affinity  
21 tag followed by a TEV cleavage site (Protex, Leicester University). The plasmids  
22 used in the electrophysiology studies were constructed as follows. TRPV6<sup>1-725</sup> and  
23 TRPV6<sup>1-725(L707A)</sup> were generated by PCR and cloned into the mammalian expression  
24 vector pCINeo/IRES-eGFP<sup>23</sup>. All constructs were sequence verified.  
25  
26  
27  
28  
29  
30  
31  
32  
33

### 34 **Protein expression and purification**

35 Proteins were expressed in *E. coli* BL21 Star (DE3) (Novagen) and purified as  
36 previously described<sup>34</sup>. Recombinant proteins were analysed by 16 % SDS-PAGE and  
37 stained using brilliant blue R-250. Protein concentration was determined at A<sub>280</sub>  
38 (Eppendorf BioPhotometer plus) using the respective extinction coefficient as  
39 determined by the ProtParam Tool (<http://web.expasy.org/protparam/>).  
40  
41  
42  
43  
44

### 45 **Analytical gel filtration**

46 Recombinant CaM and TRPV6 proteins were dialysed into gel filtration buffer (20  
47 mM Tris-Cl pH 8.0, 150 mM NaCl and 2 mM DTT). Complexes were formed in the  
48 presence of 10 mM Ca<sup>2+</sup> at room temperature for 30 minutes. Analytical gel filtration  
49 chromatography was carried out using a Superdex-75 (10/300) column (GE  
50 Healthcare) pre-equilibrated and then run in gel filtration buffer.  
51  
52  
53  
54  
55  
56  
57  
58  
59  
60

### NMR spectroscopy (sample preparation)

Recombinant CaM and TRPV6 proteins used in NMR experiments were dialysed against high-Ca<sup>2+</sup> buffer (20 mM Tris-Cl pH 7.4, 50 mM KCl and 10 mM CaCl<sub>2</sub>). All NMR samples contained 5% <sup>v/v</sup> D<sub>2</sub>O.

### NMR spectroscopy: experiments

Spectra were recorded at 308 K on Bruker 500 MHz AVI; 600 MHz AVIII; 600 MHz AVIII HD and 800 MHz AVII, with the 600 MHz and 800 MHz spectrometers equipped with CryoProbes<sup>TM</sup>. The binding of TRPV6 proteins to CaM was monitored by 2D <sup>15</sup>N-<sup>1</sup>H-HSQC experiments. Changes in the Ca<sup>2+</sup> bound status of the CaM lobes was easily visualised by the presence or absence of representative CaM N- and C-lobe peaks (cf. Fig S1A).

For the assignment of <sup>13</sup>C<sup>15</sup>N-CaM complexes with TRPV6<sup>655-722</sup>, the following series of heteronuclear triple-resonance experiments were performed: 3D HNCA, HNCACB, HN(CO)CA, CBCA(CO)NH, HNCOC, which yielded backbone and C $\beta$  chemical shift assignments. Data were analysed using CcpNmr AnalysisAssign<sup>51</sup>. CaM chemical shift perturbations (CSP) resulting from binding were calculated for individual atoms and averaged with the differences of their directly bonded neighbours using a 7:1 weighting for <sup>1</sup>H resonances vs. <sup>15</sup>N resonances.

Minimal shift mapping using a nearest-peak based approach<sup>35</sup> was performed as follows. A resonance frequency amide peak table for each mutant spectrum was generated in TopSpin3.2 (Bruker). CSPs were calculated using a weighting for <sup>1</sup>H resonances vs. <sup>15</sup>N resonances of 7:1 for all mutant spectra derived peaks relative to each assigned peak in the <sup>15</sup>N-CaM<sub>WT</sub>:TRPV6<sup>655-722</sup> wild-type spectra, with the lower limit taken as the minimal shift. This analysis was performed on the following <sup>15</sup>N-CaM<sub>WT</sub>:TRPV6 complex amide residues; CaM N-lobe residues 2-41; 44-47; 51-65; 67-70 and C-lobe residues 84-148. Thus, this analysis generates a lower limit for the CSP value of each of these backbone amide residues.

### Isothermal Titration Calorimetry (ITC)

Recombinant CaM and TRPV6 proteins used in ITC experiments were prepared as for the NMR experiments (above). The concentration of CaM in the cell ranged from 17.4-23  $\mu$ M with a 19-fold excess of TRPV6 protein in the syringe. ITC experiments

1  
2  
3 were performed using a VP-ITC MicroCalorimeter. Samples were equilibrated to 25  
4 °C, then 20 serial injections of 5  $\mu$ l were added at a stirring speed of 300 rpm at an  
5 interval of 4 minutes, followed by 19 serial injections of 10  $\mu$ l under the same  
6 conditions. To correct for background heating effects TRPV6 protein was titrated into  
7 buffer alone. ITC data analysis was carried out using Origin 7 software using either a  
8 one or two site binding model.  
9  
10  
11  
12  
13

### 14 **Electrophysiological recordings**

15 TRPV6 channel inactivation was determined by measuring the kinetics of TRPV6  
16 currents using the whole-cell configuration of the patch-clamp technique. HEK293  
17 cells were transiently transfected with pCINeo/IRES-eGFP TRPV6 using  
18 Lipofectamine 2000 (Invitrogen). After 4 hours, the transfection media was  
19 exchanged for a low  $\text{Ca}^{2+}$  DMEM culture media (to minimize inward calcium fluxes  
20 during cell culture) supplemented with 1.8 mM  $\text{MgCl}_2$  (to replace  $\text{CaCl}_2$  and keep  
21 total divalent cation concentration the same as standard culture media), 10 % serum,  
22 L-glutamine, penicillin and streptomycin. Cells were lifted off the plate using  
23 enzyme-free cell dissociation buffer (Invitrogen, UK). Cells were superfused with  
24 room temperature NMDG-based (0  $\text{Na}^+$ , 0  $\text{Ca}^{2+}$ ) extracellular solution containing 142  
25 mM NMDG-Cl, 4 mM  $\text{CsCl}$ , 1 mM  $\text{MgCl}_2$ , 10 mM Glucose, 5 mM HEPES, pH 7.4.  
26 Borosilicate glass patch-pipettes (2 – 4 M $\Omega$ ) were filled with an intracellular solution  
27 containing 100 mM Cs Aspartate, 20 mM  $\text{CsCl}$ , 4 mM  $\text{Na}_2\text{ATP}$ , 10 mM HEPES, 10  
28 mM BAPTA, 1 mM  $\text{MgCl}_2$ , pH 7.2. The recording chamber was grounded through  
29 an agar bridge connected to an Ag/AgCl pellet in 3 M  $\text{KCl}$ . A pipette offset was  
30 applied to correct for junction potentials prior to recording. Once whole cell access  
31 was achieved, cells were left for 2 mins for cell dialysis with pipette solution.  
32 Currents were elicited with 400 ms duration voltage clamp steps applied repetitively  
33 every 500 ms, from a holding potential of -20 mV to a step potential of -100 mV. To  
34 measure TRPV6 currents, the extracellular solution was switched to a 2 mM  $\text{CaCl}_2$ ,  
35 140 mM  $\text{NaCl}$ -based ( $\text{Ca}^{2+} + \text{Na}^+$ ) solution (all other components were the same as  
36 the NMDG-solution). Leak current was measured prior to the extracellular solution  
37 being exchanged for a 2 mM  $\text{Ca}^{2+}$ ,  $\text{NaCl}$  based (control) solution. Currents were  
38 sampled at 5 kHz and recorded to disk for off-line analysis. TRPV6 currents were  
39 measured as the peak current in  $\text{Ca}^{2+} + \text{Na}^+$  solution, minus current in the NMDG  
40  
41  
42  
43  
44  
45  
46  
47  
48  
49  
50  
51  
52  
53  
54  
55  
56  
57  
58  
59  
60

1  
2  
3 solution. PClamp9 software (Molecular Devices) was used for data acquisition and  
4 current trace analysis and Prizm (Graphpad) for figure preparation and statistical  
5 analysis. Experimental traces did not decay exponentially and consequently were best  
6 described by time analysis at 20, 50 and 80 % inactivation.  
7  
8  
9

## 10 11 **Results**

### 12 ***TRPV6 is bound to the CaM<sub>C</sub> lobe to form the resting Ca<sup>2+</sup>-open state***

13  
14 We previously targeted the cytoplasmic TRPV6 C-tail (residues 579-725) and  
15 identified the TRPV6<sup>691-716</sup> C-tail peptide as a high-affinity CaM binder ( $K_d$  of  $77 \pm$   
16  $18$  nM) under a  $\sim 100$ -fold excess of Ca<sup>2+</sup> (high-Ca<sup>2+</sup> conditions)<sup>24</sup>. To investigate  
17 both the Ca<sup>2+</sup> dependency and CaM-lobe specificity of the CaM:TRPV6 C-tail  
18 interaction, we selected the longest soluble TRPV6 region of 655-722<sup>25</sup>. This  
19 fragment was used in conjunction with a set of previously described CaM mutants  
20 which have impaired Ca<sup>2+</sup> binding properties in one or more of CaM's Ca<sup>2+</sup> binding  
21 sites (Fig S1A)<sup>36</sup>. In particular, we used variants which prevent either the N-lobe, the  
22 C-lobe or both lobes from binding Ca<sup>2+</sup>. Following convention, these were denoted as  
23 CaM<sub>12</sub>, CaM<sub>34</sub>, and CaM<sub>1234</sub>, respectively, where the subscripts indicate the mutation  
24 of the relevant CaM Ca<sup>2+</sup>-binding sites. The structural integrity of the mutant CaMs  
25 was confirmed by analysis of <sup>15</sup>N-<sup>1</sup>H-HSQC spectra, where changes in the Ca<sup>2+</sup> bound  
26 status of the individual CaM lobes can be readily visualised by the presence of peaks  
27 corresponding to residues in each lobe (Figs S1B-I).  
28  
29  
30  
31  
32  
33  
34  
35  
36

37 Analysis of the binding of TRPV6<sup>655-722</sup> to the various Ca<sup>2+</sup> deficient CaM<sub>12</sub>,  
38 CaM<sub>34</sub> and CaM<sub>1234</sub> mutants under high-Ca<sup>2+</sup> [10mM] conditions using analytical gel  
39 filtration and NMR spectroscopy revealed that disruption of all four Ca<sup>2+</sup> binding sites  
40 in CaM (CaM<sub>1234</sub>) was sufficient to abrogate virtually all binding (Fig. S2A,B).  
41 Disruption of Ca<sup>2+</sup> binding to the CaM C-lobe in the CaM<sub>34</sub> protein, which is defunct  
42 in its Ca<sup>2+</sup> binding to the C-lobe but has native Ca<sup>2+</sup>-binding capability for its N-lobe,  
43 also resulted in no significant interaction with the TRPV6 C-tail by analytical gel  
44 filtration (Fig. S2C) but CaM N-lobe specific shifts were observed in the <sup>15</sup>N-<sup>1</sup>H-  
45 HSQC spectrum (Fig. S2D), suggestive of a weak binder. In contrast, Ca<sup>2+</sup> bound  
46 CaM<sub>12</sub>, which has Ca<sup>2+</sup> bound only to the CaM C-lobe was sufficient to facilitate  
47 strong TRPV6<sup>655-722</sup> binding, as evident from gel filtration (Fig. 1A), NMR  
48 spectroscopy (Fig. 1B) and ITC (Fig. 1C). The CaM<sub>12</sub>-TRPV6 complex displayed a  
49  $\sim 1:1$  stoichiometry with a  $K_d$  of  $34 \pm 3$  nM indicative of a tight binding event.  
50  
51  
52  
53  
54  
55  
56  
57  
58  
59  
60

Weighted average chemical shift perturbations (CSPs, Fig 1D), which yield residue-specific information regarding the binding event, are observed exclusively for residues in the Ca<sup>2+</sup>-loaded C-lobe. Notably, the largest CSPs were observed for residues F92 and M144, which together make up a substantial part of the well-characterised hydrophobic pocket of the CaM C-lobe that is formed upon binding Ca<sup>2+</sup><sup>37</sup> and fully consistent with the structure of the CaM<sub>12</sub>:TRPV5<sup>655-725</sup> complex<sup>52</sup>.

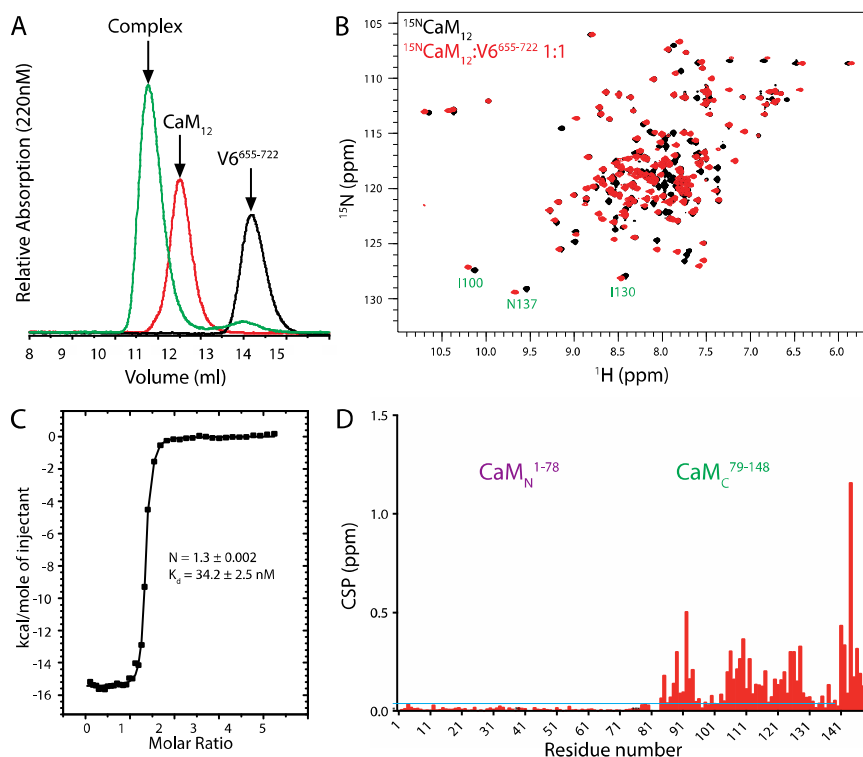


Figure 1- Analysis of TRPV6 C-tail binding to the Calmodulin N-lobe (CaM<sub>12</sub>).

A) Analytical gel filtration curves are displayed for; free TRPV6<sup>655-722</sup> in black, free CaM<sub>12</sub> in red and the corresponding CaM<sub>12</sub>:TRPV6<sup>655-722</sup> complex at a 1:1 molar ratio in green.

B) Overlay of the <sup>15</sup>N-<sup>1</sup>H-HSQC spectra of <sup>15</sup>N-labelled CaM<sub>12</sub> (black) with the <sup>15</sup>N-labelled CaM<sub>12</sub>:TRPV6<sup>655-722</sup> complex (red) at a 1:1 molar ratio. Note that non-overlapping peaks identify residues affected by complex formation.

C) Representative ITC plot of CaM<sub>12</sub> titrated by TRPV6<sup>655-722</sup> and fitted using the one binding site model. Values for the number of binding sites N, together with the binding constant K<sub>d</sub> are shown. Number of replicates equals 3.

D) CaM<sub>12</sub> chemical shift perturbation (CSP) ( $\delta_{\text{bound}} - \delta_{\text{free}}$ ) as a function of residue number for the <sup>15</sup>N-labelled CaM<sub>12</sub>:TRPV6<sup>655-722</sup> complex at a molar ratio of 1:1. CSP values (ppm) were calculated as described in the materials and methods. A horizontal light blue line indicates the estimated absolute error.

1  
2  
3 We also tested the effect of the individual  $\text{Ca}^{2+}$ -binding sites in the CaM C-lobe using  
4 the CaM<sub>123</sub> and CaM<sub>124</sub> mutants to conclude that  $\text{Ca}^{2+}$  binding to site 4 in CaM is  
5 essential for the interaction with TRPV6 (Fig. S3). For the paralogue TRPV5 we also  
6 clearly established that a specific CaM:TRPV5 complex is formed under cellular  
7 basal  $\text{Ca}^{2+}$  conditions that involves a fully  $\text{Ca}^{2+}$ -loaded CaM C-lobe<sup>52</sup> and hence, by  
8 analogy we infer the same molecular state for the CaM:TRPV6 complex.  
9  
10

11  
12 Thus, based on these combined data we propose that, induced by the  
13 differential affinities of the CaM C- and N-lobes for  $\text{Ca}^{2+}$ , CaM first binds to the  
14 TRPV6 C-tail via critical contacts made solely within a fully  $\text{Ca}^{2+}$ -loaded C-lobe.  
15  
16  
17

### 18 19 ***Elevated $\text{Ca}^{2+}$ switches TRPV6 to a high $\text{Ca}^{2+}$ -open state mediated via CaM N-lobe*** 20 ***specific interactions*** 21

22 To further investigate the role of the CaM N-lobe in  $\text{Ca}^{2+}$ -mediated TRPV6  
23 channel inactivation, we next assessed the interaction between TRPV6<sup>655-722</sup> and CaM  
24 under high- $\text{Ca}^{2+}$  (10mM) conditions. Analysis of this interaction by ITC (Fig. 2A)  
25 revealed an initial tight binding event with a  $K_d$   $43 \pm 11$  nM, similar to that previously  
26 seen for CaM<sub>12</sub> (cf. Fig. 1C). However, unlike the interaction of TRPV6 with CaM<sub>12</sub>,  
27 in the presence of a  $\text{Ca}^{2+}$ -loaded CaM N-lobe, a second weaker interaction (9  $\mu\text{M}$ ) is  
28 also evident suggesting a two-step binding pattern (*vide infra*). NMR spectroscopy  
29 (Figs 2B,C) revealed that both CaM N- and CaM C-lobes now engage the TRPV6 C-  
30 tail, in marked contrast to the low- $\text{Ca}^{2+}$  state exemplified by the CaM<sub>12</sub>-TRPV6  
31 complex. To determine which CaM residues are involved in the transition from the  
32 resting-open state (CaM<sub>12</sub>:TRPV6<sup>655-722</sup>) to the high- $\text{Ca}^{2+}$  open-state  
33 (CaM<sub>WT</sub>:TRPV6<sup>655-722</sup>), we subtracted the CSPs for CaM<sub>12</sub>:TRPV6<sup>655-722</sup> (Fig. 1D)  
34 from those obtained for CaM<sub>WT</sub>:TRPV6<sup>655-722</sup> (Fig. 2C), effectively yielding the  
35 differential effects between the two complexes. The results of this analysis (Fig. 2D)  
36 clearly show that the major effects occur for CaM N-lobe residues with only minor  
37 changes observed for residues in the CaM C-lobe. In addition, the largest changes for  
38 the C-lobe occur for residues close in sequence to the N-lobe and are therefore likely  
39 due to their physical proximity to the N-lobe, rather than to a change in actual  
40 binding.  
41  
42  
43  
44  
45  
46  
47  
48  
49  
50  
51  
52  
53  
54  
55  
56  
57  
58  
59  
60

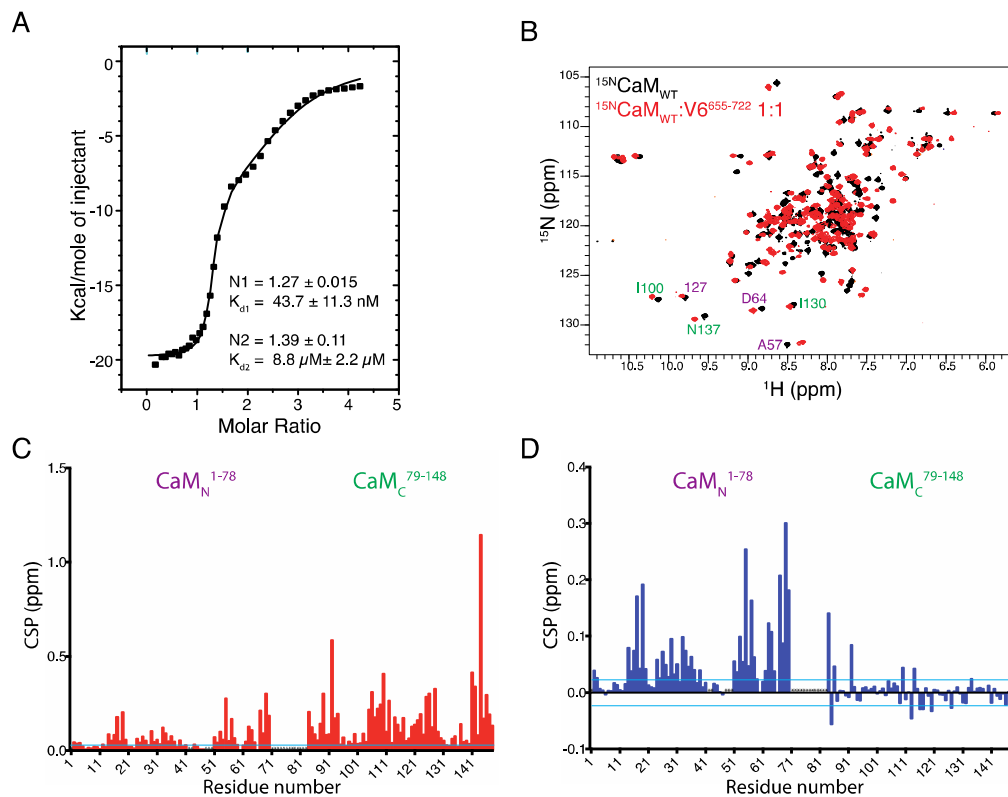


Figure 2- Analysis of TRPV6 C-tail binding to the fully  $\text{Ca}^{2+}$ -loaded Calmodulin (CaM<sub>WT</sub>).

A) Representative ITC plot of CaM<sub>WT</sub> titrated by TRPV6<sup>655-722</sup> and fitted using a two sites model. Values for the number of binding sites  $N$ , together with the binding constant  $K_d$  are shown. Number of replicates equals 3.

B) Overlay of the  $^{15}\text{N}$ - $^1\text{H}$ -HSQC spectra of  $^{15}\text{N}$ -labelled CaM<sub>WT</sub> (black) and the  $^{15}\text{N}$ -labelled CaM<sub>WT</sub>:TRPV6<sup>655-722</sup> complex (red) at a 1:1 molar ratio.

C) CaM<sub>WT</sub> chemical shift perturbations (CSPs) ( $\delta_{\text{bound}} - \delta_{\text{free}}$ ) as a function of residue number for the  $^{15}\text{N}$ -labelled CaM<sub>WT</sub>:TRPV6<sup>655-722</sup> complex at a molar ratio of 1:1. CSP values (ppm) were calculated as described in the materials and methods.

D) CSP differences of the 1:1 CaM<sub>WT</sub>:TRPV6<sup>655-722</sup> complex (as in C) and the 1:1 CaM<sub>12</sub>:TRPV6<sup>655-722</sup> complex (cf. Fig. 2D) as a function of residue number. Horizontal light blue lines in C) and D) indicate the estimated absolute error.

1  
2  
3 To date, the CaM:TRPV1<sup>767-801</sup> represents the only CaM:TRP C-tail complex  
4 for which an atomic structure has been solved (PDB id 3SUI; Fig. 3A)<sup>38</sup>. Under high  
5 Ca<sup>2+</sup> conditions, CaM:TRPV1<sup>767-801</sup> adopts the typical closed canonical fold observed  
6 in many CaM:peptide complexes<sup>32</sup>. Further analysis of the structure of this complex  
7  
8  
9  
10  
11  
12  
13  
14  
15  
16  
17  
18  
19  
20  
21  
22  
23  
24  
25  
26  
27  
28  
29  
30  
31  
32  
33  
34  
35  
36  
37  
38  
39  
40  
41  
42  
43  
44  
45  
46  
47  
48  
49  
50  
51  
52  
53  
54  
55  
56  
57  
58  
59  
60

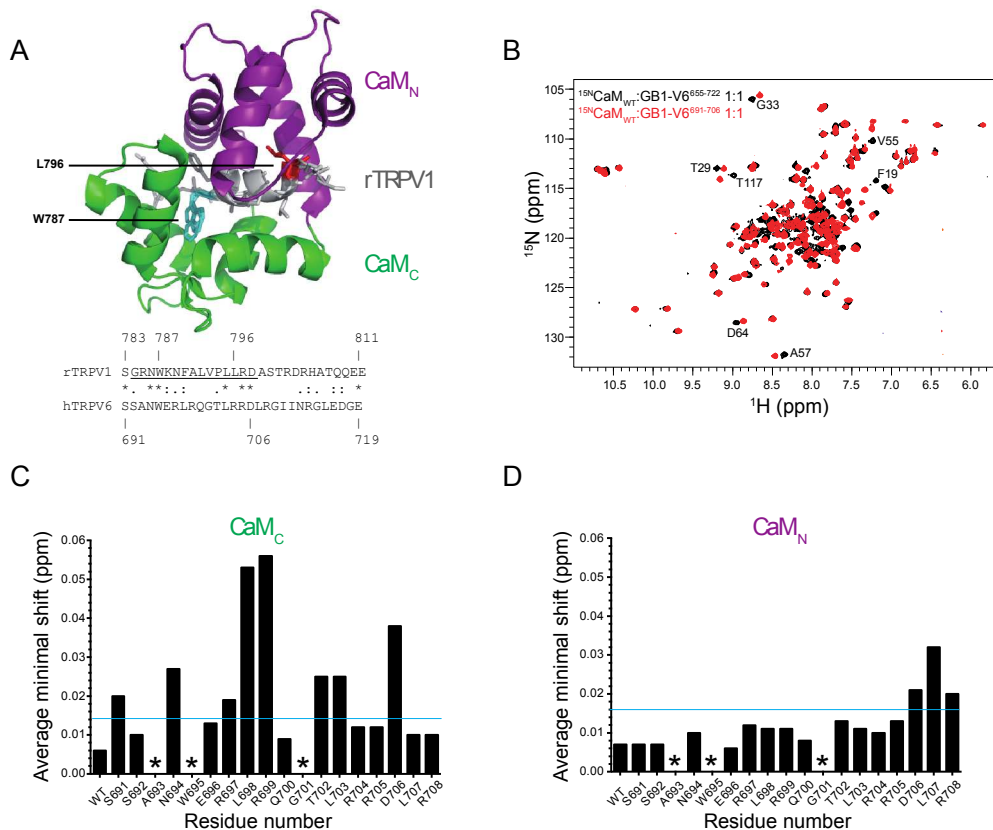


Figure 3- Analysis of the TRV6 C-tail CaM binding site.

A) Ribbon diagram of the crystal structure of the CaM:rTRPV1<sup>767-801</sup> C-tail complex (PDB: 3SUI)<sup>36</sup>. The CaM N-lobe (purple), C-lobe (green) and the rTRPV1 peptide (grey) are indicated. Key rTRPV1 CaM N- and C-lobe residues are highlighted. Below: pairwise alignment between the rTRPV C-tail CaM binding region and the analogous region of TRPV6. The rTRPV1 region present in the crystal structure in (A) is underlined.

B) Overlay of the <sup>15</sup>N-<sup>1</sup>H-HSQC spectra of the 1:1 <sup>15</sup>N-labelled CaM<sub>WT</sub>:GB1-TRPV6<sup>655-722</sup> complex (black) with the 1:1 <sup>15</sup>N-labelled CaM<sub>WT</sub>:GB1-TRPV6<sup>691-706</sup> complex (red).

C) Alanine scanning mutagenesis of the TRPV6<sup>655-722</sup> C-tail CaM binding site. <sup>15</sup>N-labelled CaM:mutant TRPV6<sup>655-722</sup> 1:1 complexes were analysed by <sup>15</sup>N-<sup>1</sup>H-HSQC NMR. Each bar represents the average of the minimal shift CSPs for the CaM<sub>C</sub> lobe region, calculated as described in the materials and methods. Untested residues are labelled with an asterisk. A horizontal light blue bar indicates the estimated absolute error for the <sup>15</sup>N-labelled CaM:TRPV6<sup>655-722</sup> 1:1 complex.

D) As for C) but calculated for the CaM<sub>N</sub> lobe.

shows that the minimal TRPV1 CaM-interacting region comprises residues 784-798. In order to compare this CaM interacting region to the analogous 691-706 region within the TRPV6 fragment, we assembled the 1:1 <sup>15</sup>N-CaM<sub>WT</sub>:TRPV6<sup>GB1-655-722</sup> and 1:1 <sup>15</sup>N-CaM<sub>WT</sub>:TRPV6<sup>GB1-691-706</sup> complexes. Comparison of their <sup>15</sup>N-<sup>1</sup>H-HSQC

1  
2  
3 spectra (Fig. 3B) clearly indicates that residues outside of TRPV6 691-706 are also  
4 involved in this interaction. Furthermore, a qualitative analysis suggested that the  
5 differential effects predominantly involve residues specific to the CaM N-lobe, which  
6 can only be rationalised by a complex that is structurally distinct from the  
7 CaM:TRPV1 complex.  
8  
9

10  
11 To assess the contributions of individual TRPV6 residues to lobe-specific  
12 CaM binding in the context of the longer C-tail fragment (655-722), we employed  
13 alanine-scanning mutagenesis. We excluded W695 as this residue has previously been  
14 shown to fully abrogate CaM binding<sup>18</sup>. The ability of each TRPV6 mutant protein to  
15 bind to <sup>15</sup>N-CaM<sub>WT</sub> under high Ca<sup>2+</sup> conditions was assessed by <sup>15</sup>N-<sup>1</sup>H-HSQC and  
16 the data analysed using a minimal shift or nearest neighbour approach; this  
17 methodology has been shown to accurately reflect protein-protein interactions<sup>35,39</sup>.  
18 Minimal shift analyses of fifteen <sup>15</sup>N-CaM<sub>WT</sub>:TRPV6 mutant protein complexes are  
19 shown in Fig. S4 with the mean shifts for the CaM C- and N-lobes presented in Figs  
20 3C and 3D, respectively. Three distinct parts to the TRPV6 CaM binding region can  
21 be identified: a CaM C-lobe specific region comprised of residues S691-L703, a CaM  
22 N-lobe specific region encompassing residues L707-R708 and a hinge region formed  
23 by D706. Furthermore, this CaM:TRPV6 binding pattern suggests that, unlike  
24 TRPV1, under high-Ca<sup>2+</sup> conditions TRPV6 induces a different CaM complex in  
25 which interactions occur independently across both CaM lobes.  
26  
27

28  
29 In summary, the data show that in response to increasing [Ca<sup>2+</sup>] the CaM N-  
30 lobe becomes fully loaded with Ca<sup>2+</sup>, in which the CaM:TRPV6 complex is  
31 characterised by CaM N-lobe specific interactions with the C-terminal portion of the  
32 TRPV6 CaM binding site.  
33  
34

### 35 ***TRPV6 is inactivated by CaM<sub>WT</sub> via a novel two-tail mechanism***

36  
37 The ITC data probing the interaction between TRPV6<sup>655-722</sup> and CaM<sub>WT</sub> (Fig.  
38 2A) showed the presence of a second weaker binding event, such that one CaM<sub>WT</sub> can  
39 bind two TRPV6<sup>655-722</sup> moieties. NMR spectroscopy of the CaM<sub>WT</sub> and TRPV6<sup>655-722</sup>  
40 complexes at 1:1 and 1:2 molar ratios (Figs 4A,B) showed that significant changes  
41 arising from the binding of the second TRPV6 moiety are almost exclusively  
42 observed for the CaM N-lobe. Interestingly, the most affected residues are part of the  
43 hydrophobic pocket on the N-lobe (Fig. 4C), which is formed when it binds Ca<sup>2+</sup><sup>37</sup>.  
44  
45  
46  
47  
48  
49  
50  
51  
52  
53  
54  
55  
56  
57  
58  
59  
60

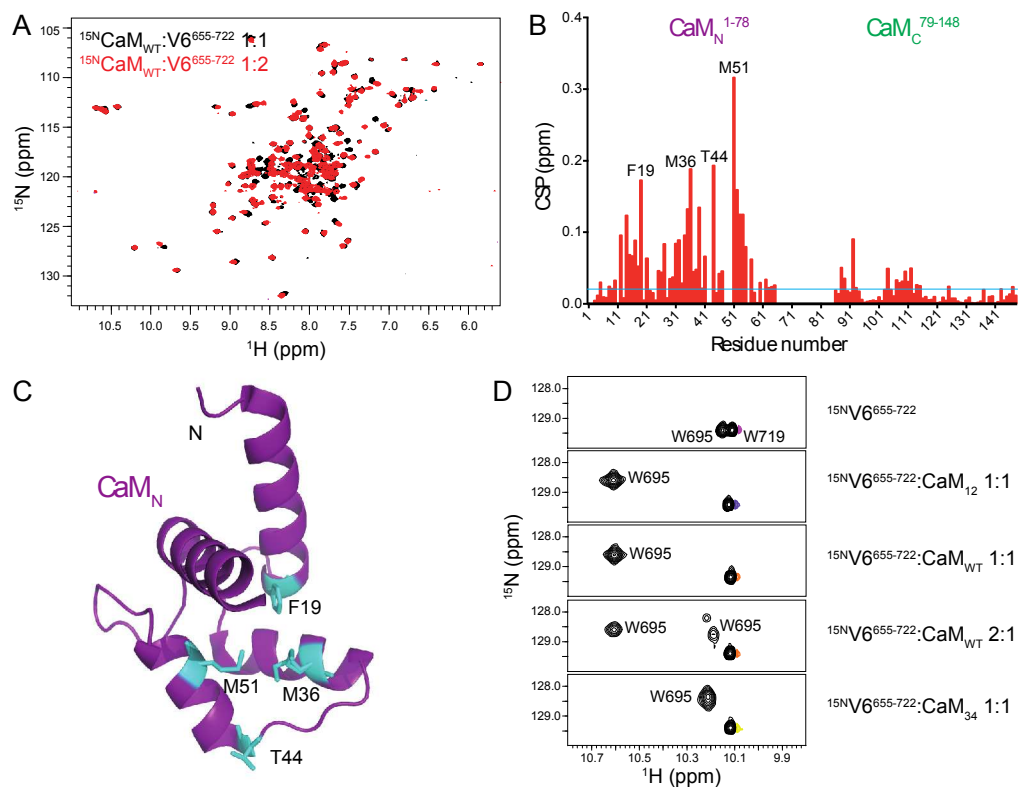


Figure 4- Analysis of the second TRV6 C-tail CaM binding site.

A) Overlay of the  $^{15}\text{N}$ - $^1\text{H}$ -HSQC CaM spectra of the 1:1  $^{15}\text{N}$ -labelled CaM<sub>WT</sub>:TRPV6<sup>655-722</sup> complex (black) with the 1:2  $^{15}\text{N}$ -labelled CaM<sub>WT</sub>:TRPV6<sup>655-722</sup> complex (red).

B) CaM<sub>WT</sub> chemical shift perturbation (CSP) ( $\delta_{\text{bound } 1:2} - \delta_{\text{bound } 1:1}$ ) as a function of residue number for the 1:2  $^{15}\text{N}$ -labelled CaM<sub>WT</sub>:TRPV6<sup>655-722</sup> complex compared to the 1:1 complex. CSP values (ppm) were calculated as described in the materials and methods. The horizontal light blue line indicates the estimated absolute error. The four residues with the largest CSPs are highlighted.

C) Ribbon diagram of the CaM N-lobe (purple) of the CaM:rTRPV1<sup>767-801</sup> C-tail complex (PDB: 3SUI)<sup>36</sup>. Highlighted residues from B) are shown as sticks (cyan).

D) Zoomed regions of various  $^{15}\text{N}$ - $^1\text{H}$ -HSQC spectra of  $^{15}\text{N}$ -labelled TRPV6<sup>655-722</sup> in complex with different Ca<sup>2+</sup> bound forms of CaM. The indole ring amino group of the tryptophan side chains for residues W695 and W719 are marked.

We then assessed the role of W695 in formation of the 1:2 complex. Two tryptophan residues are present in the TRPV6<sup>655-722</sup> construct; W695 and W719, whose side-chain indole amino groups present convenient probes to monitor the interaction by recording  $^{15}\text{N}$ - $^1\text{H}$ -HSQC spectra of  $^{15}\text{N}$ -TRPV6<sup>655-722</sup> and its various CaM complexes (Fig. 4D). As expected neither CaM<sub>WT</sub>, nor the various mutant CaMs, affect the W719 cross-peak, consistent with the notion that this residue does not participate in binding. However, the cross-peak of W695 is strongly shifted upon

1  
2  
3 addition of CaM<sub>12</sub>, binding to the CaM C-lobe in line with its proposed crucial role in  
4 complex formation<sup>18</sup> and the CaM<sub>12</sub>:TRPV5 structure<sup>52</sup>. Conversely, a unique cross  
5 peak position is observed for the 1:1 CaM<sub>34</sub>:<sup>15</sup>N-TRPV6<sup>655-722</sup> complex, in which  
6 only the CaM N-lobe is Ca<sup>2+</sup>-bound and engages with the TRPV6<sup>655-722</sup> moiety.  
7 Comparison of the 1:1 CaM<sub>12</sub>:<sup>15</sup>N-TRPV6<sup>655-722</sup> complex with the 1:1 CaM<sub>WT</sub>:<sup>15</sup>N-  
8 TRPV6<sup>655-722</sup> complex shows an identical pattern for both complexes, indicating that  
9 W695 is bound to the CaM C-lobe in both instances. Interestingly, upon formation of  
10 the 1:2 CaM<sub>WT</sub>:<sup>15</sup>N-TRPV6<sup>655-722</sup> complex, a W695 cross-peak appears at a spectral  
11 location similar to the cross-peak observed for the 1:1 CaM<sub>34</sub>:<sup>15</sup>N-TRPV6<sup>655-722</sup>  
12 complex. Thus, we conclude that in the 1:2 CaM<sub>WT</sub>:<sup>15</sup>N-TRPV6<sup>655-722</sup> complex one  
13 TRPV6 tail is bound to the CaM C-lobe via its W695 residue, while a second TRPV6  
14 C-tail is bound to the CaM N-lobe via its W695 residue.  
15  
16  
17  
18  
19  
20  
21

22 To further investigate the role of the critical TRPV6-CaM N-lobe interactions  
23 on channel inactivation we decided to focus on the L707 residue, which we identified  
24 as a CaM N-lobe specific interactor from the alanine scanning mutagenesis (Figs 3C-  
25 D). Therefore, we evaluated the binding of the TRPV6<sup>655-722</sup> L707A mutant to CaM<sub>WT</sub>  
26 by NMR spectroscopy (Figs 5A, B) and ITC (Fig. 5C). CSP analysis shows changes  
27 predominantly for residues in the CaM<sub>WT</sub> N-lobe, with minor changes seen for the C-  
28 lobe residues closest to the N-lobe. The latter probably arise indirectly from a  
29 proximity effect. Interestingly, the most-affected residues cluster in the hydrophobic  
30 pocket (Fig. 5B) also identified for the 2;1 interaction. The mutation has increased the  
31 affinity of TRPV6<sup>655-722</sup> L707A for CaM<sub>WT</sub> for the first binding event by ~2-fold, but  
32 significantly, increased the affinity of the second binding event by 10-fold.  
33  
34  
35  
36  
37  
38  
39

40 If the formation of the 1:2 complex has a functional role, the increased affinity  
41 of the second binding event resulting from the L707A mutation would be expected to  
42 stabilise the inactivated state and thus increase the rate of channel inactivation. Hence,  
43 the effect of the L707A mutation in the context of the intact channel was investigated  
44 by measuring channel inactivation in mammalian cells. TRPV6 mediated currents  
45 were recorded by whole-cell voltage clamp in HEK293 cells expressing either WT or  
46 mutant L707A channels. We ensured proper control of intra-cellular Ca<sup>2+</sup> during cell  
47 culturing and experiment preparation (see methods) and leak currents were measured  
48 prior to the extracellular solution being exchanged for high Ca<sup>2+</sup> conditions.  
49  
50  
51  
52  
53  
54  
55  
56  
57  
58  
59  
60

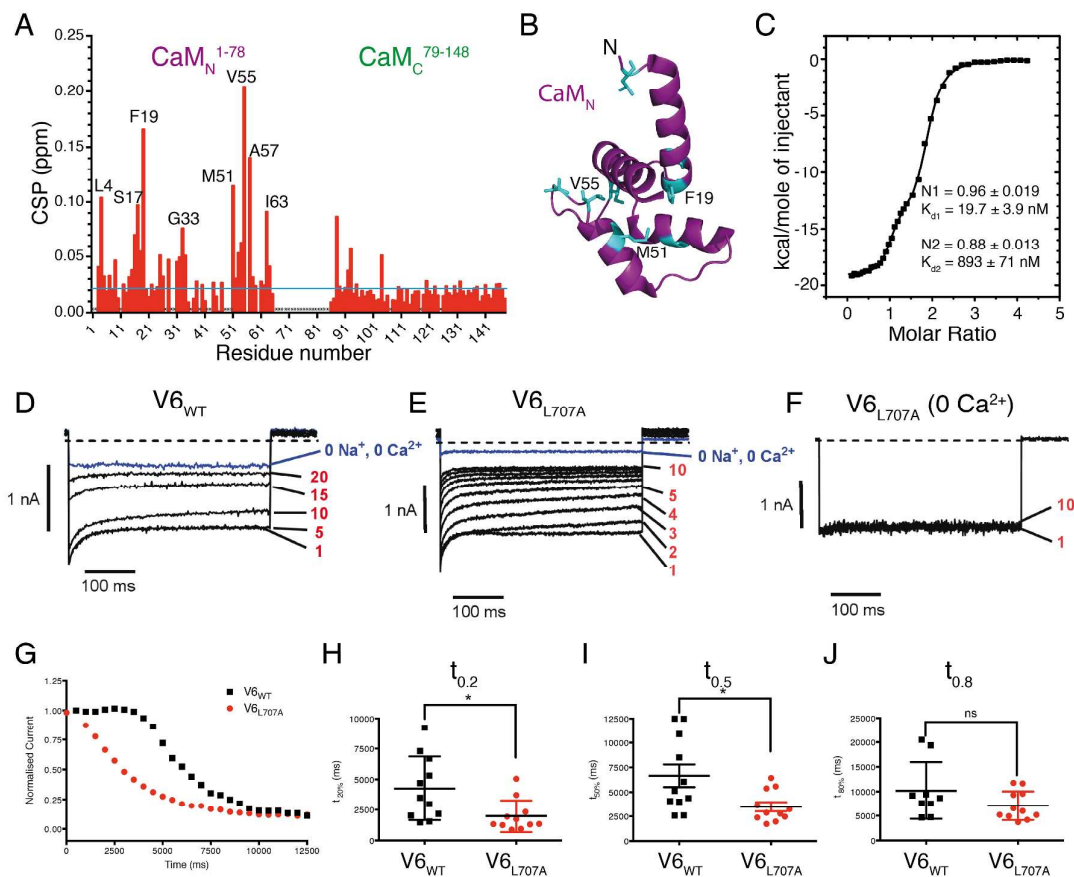


Figure 5- Characterisation of the TRPV6<sup>655-722</sup> L707A mutant.

A) CaM<sub>WT</sub> chemical shift perturbation (CSP) ( $\delta_{\text{boundV6L707A}} - \delta_{\text{boundV6WT}}$  1:1) as a function of residue number for the 1:1 <sup>15</sup>N-labelled CaM<sub>WT</sub>-TRPV6<sup>655-722(L707A)</sup> mutant complex. CSP values (ppm) were calculated as described in the materials and methods. A horizontal light blue line indicates the estimated absolute error. Residues with the largest CSP are highlighted.

B) Ribbon diagram of the CaM N-lobe (purple) of the CaM:rTRPV1<sup>767-801</sup> C-tail complex (PDB: 3SUI). Highlighted residues from A) are shown as sticks (cyan).

C) Representative ITC plot of CaM<sub>WT</sub> titrated by the TRPV6<sup>655-722(L707A)</sup> mutant and fitted using the two sites model. Values for the number of binding sites N, together with the binding constant  $K_d$  are shown. Number of replicates equals 2.

D-E) Representative WT (D) and L707A (E) TRPV6 whole cell current traces elicited by repetitively pulsing to 100 mV. Currents were first recorded in an NMDG-based (0 Na<sup>+</sup>, 0 Ca<sup>2+</sup>) solution, then switched to a normal Na<sup>+</sup> + Ca<sup>2+</sup> based solution. For clarity, only selected traces, different for each panel, are shown with the corresponding pulse number indicated to the right of each panel. Note that WT currents are superimposed for the first 5 pulses, whereas L707A currents decrease substantially during the same time-frame.

F) Representative L707A TRPV6 whole cell current recordings from a cell perfused with 0 Ca<sup>2+</sup> (0 mM Ca<sup>2+</sup>, 2 mM EGTA) NaCl-based extracellular solution. Currents showed no fast or slow components of inactivation in the absence of extracellular Ca<sup>2+</sup> (for clarity, only first 10 current traces are shown).

1  
2  
3 (G) Representative time courses of  $\text{Ca}^{2+}$ -dependent current inactivation for WT and L707A TRPV6  
4 currents. Peak currents with each voltage pulse were normalised to peak current at pulse 1 and plotted  
5 against time. Each symbol represents normalised current from a single voltage pulse.

6  
7 (H-J) Time to 20, 50 and 80 % inactivation. Each symbol is a measure from a single cell. Horizontal  
8 lines indicate mean  $\pm$  SEM. \*  $p < 0.05$ . ns – not significant.  
9

10  
11 Representative TRPV6 and TRPV6 L707A currents recorded in control  
12 solutions in response to 500 ms repetitive pulsing to -100 mV at a frequency of 1 Hz  
13 are shown in Figs 5D-E. As reported previously<sup>18,40</sup>, two components of inactivation  
14 were observed, a rapid onset component (complete in  $\sim 50$  ms) and a slow component.  
15 Whereas the fast component rapidly recovered between pulses, after an initial delay  
16 the slow component resulted in a progressive reduction of current amplitude with  
17 repetitive pulsing (Fig. 5G). Currents could also be observed to slowly and fully  
18 recover from inactivation over a period of several minutes under conditions of  
19 reduced  $\text{Ca}^{2+}$  entry (50 ms duration pulses applied at 10 s intervals; data not shown)  
20 and inactivation was abolished in solutions without extracellular  $\text{Ca}^{2+}$  (Fig. 5F),  
21 indicating that both components of inactivation were  $\text{Ca}^{2+}$  dependent and current run-  
22 down was minimal. Mean maximum inactivation for TRPV6 and TRPV6-L707 was  
23  $86 \pm 3$  % ( $n=10$ ) and  $90 \pm 1.6$  % ( $n=12$ ), respectively. Figs 5G-I show that  
24 inactivation of TRPV6 L707A currents was significantly faster when compared to  
25 TRPV6. The mean times to 20% ( $t_{0.2}$ ) and 50% ( $t_{0.5}$ ) inactivation were  $4300 \pm 790$  ms  
26 and  $6600 \pm 1100$  ms, respectively, for TRPV6. These were significantly reduced to  
27  $1990 \pm 390$  ms and  $3500 \pm 480$  ms, respectively, for TRPV6 L707A (Figs 5H, I).  
28 Mean current amplitudes of TRPV6 L707A were  $-1600 \pm 200$  pA ( $n=11$ ), which was  
29 significantly higher than  $-1050 \pm 100$  pA ( $n=11$ ) for TRPV6. We considered the  
30 possibility that the faster inactivation of TRPV6 L707A was due to larger currents and  
31 greater  $\text{Ca}^{2+}$  influx. However, the correlation between current amplitude and  $t_{0.5}$   
32 inactivation for the combined TRPV6 and TRPV6 L707A data was poor (Pearson  $R^2$   
33 value 0.46,  $n = 22$ ) and even lower for the TRPV6 L707A data alone (Pearson  $R^2$   
34 value 0.23,  $n = 11$ ). Thus, we conclude that the TRPV6 L707A mutation increases the  
35 rate of inactivation of functional channels in a manner consistent with the effects of  
36 this mutation on CaM binding affinity.  
37  
38  
39  
40  
41  
42  
43  
44  
45  
46  
47  
48  
49  
50  
51  
52  
53  
54  
55  
56  
57  
58  
59  
60

## Discussion

The epithelial TRPV5 and TRPV6  $\text{Ca}^{2+}$ -channels play an important role in  $\text{Ca}^{2+}$  homeostasis, and their functioning is tightly controlled by a  $\text{Ca}^{2+}$ -dependent feedback mechanism(s) to facilitate channel inactivation. Calcium CaM-dependent TRPV6 channel inactivation involves the very C-terminal part of the channel, which is unfortunately either absent or unresolved in the atomic resolution structures of TRPV6<sup>8,9</sup>. Here, we have used a range of biophysical techniques to characterise the interactions of CaM with the TRPV6 C-terminal tail that underpin the mechanism of channel inactivation. We deduce that this mechanism involves three distinct states of the CaM:TRPV6 complex and propose a so-called “two-tail” model to rationalise our findings (cf. Fig. 6): The model comprises: 1) a “resting  $\text{Ca}^{2+}$ -open state” formed under basal cellular  $[\text{Ca}^{2+}]$  of  $\sim 100$  nM where calmodulin (CaM) engages the C-tail via CaM C-lobe interactions and the CaM N-lobe is in an apo state; 2) a “high- $\text{Ca}^{2+}$  open-state” is formed when an increased cellular  $[\text{Ca}^{2+}]$  loads the apo CaM N-lobe with  $\text{Ca}^{2+}$  and the C-tail can now engage the CaM N-lobe via a crucial TRPV6<sup>L707</sup>:CaM N-lobe specific interaction; 3) a “high- $\text{Ca}^{2+}$  inactivated state” is formed when the channel engages CaM via a novel mechanism, whereby a second C-tail displaces the first C-tail from the CaM N-lobe to form a complex which bridges

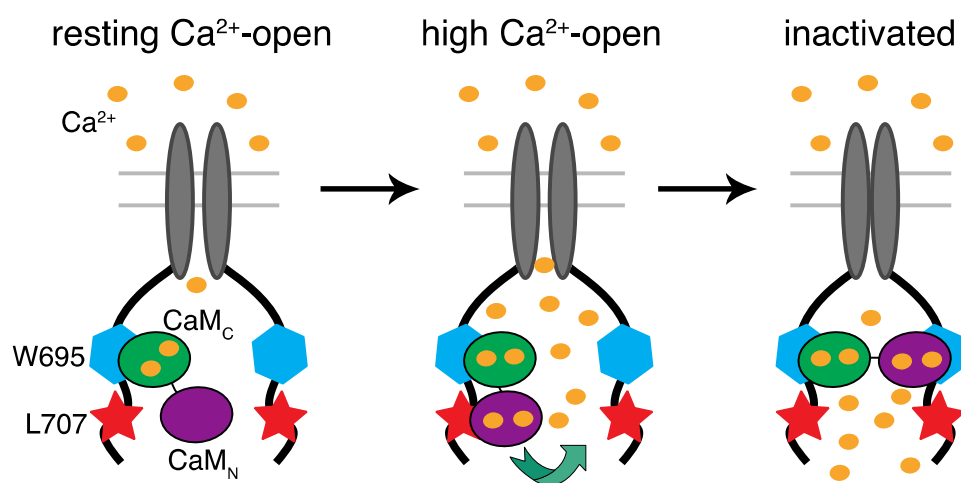


Figure 6- Schematic of the “two-tail” model of CaM-mediated TRPV regulation. Note only two of the four TRPV channel subunits are represented. Differential C- or N-lobe dependent interactions (indicated) characterise the resting  $\text{Ca}^{2+}$ -open, high  $\text{Ca}^{2+}$ -open and inactivated states. Leucine 707 is crucial in the switch to the 1:2 CaM:TRPV6 complex that results in an inactivated channel.

1  
2  
3 between two monomers and is coupled to closure of the channel pore.

4 Our data show that the low  $\text{Ca}^{2+}$ -mimicking  $\text{CaM}_{12}$ -mutant forms a tight  
5 complex mediated by only the CaM C-lobe (Fig. 1) and under resting intracellular  
6  $\text{Ca}^{2+}$  levels ( $\sim 100$  nM) the C-tail of the TRPV6 paralogue, TRPV5, is constitutively  
7 bound to  $\text{CaM}^{52}$ . Moreover, under these conditions the CaM C-lobe is fully  $\text{Ca}^{2+}$   
8 loaded whilst the N-lobe remains  $\text{Ca}^{2+}$  free. This is in line with previous  
9 observations, which showed that in HEK293 cells at an intracellular  $[\text{Ca}^{2+}]$  of 200 nM  
10 none of the  $\sim 10$   $\mu\text{M}$  total cellular CaM is fully  $\text{Ca}^{2+}$ -loaded<sup>41</sup>. In addition, a TRPV1-  
11 CaM complex was successfully purified from HEK293 cells using  
12 immunoprecipitation experiments<sup>28</sup>, also indicating a tight association between the  
13 channel and CaM under native conditions. Furthermore, live-cell FRET experiments  
14 of voltage-gated  $\text{Ca}^{2+}$  ion channels showed constitutive association of CaM with the  
15 channel under a low intracellular  $[\text{Ca}^{2+}]$ <sup>42</sup>. However in contrast, live-cell FRET  
16 experiments of TRPV6 suggested a  $[\text{Ca}^{2+}]$ -dependent association of the channel with  
17 CaM, rather than a constitutive one<sup>17</sup>. In these latter experiments, the fluorophore was  
18 tagged on to the N-terminus of the CaM N-lobe and therefore was most likely  
19 monitoring the induced association of the CaM N-lobe with the channel, as postulated  
20 by our high- $\text{Ca}^{2+}$  open-state 1:1 CaM:TRPV6 complex, rather than a direct CaM C-  
21 lobe mediated channel interaction.  
22  
23  
24  
25  
26  
27  
28  
29  
30  
31  
32

33 In direct response to elevated  $[\text{Ca}^{2+}]$  CaM is further  $\text{Ca}^{2+}$ -loaded at its N-lobe,  
34 thus extending the high affinity binding surface to include both the C- and N-lobes.  
35 This establishes the high- $\text{Ca}^{2+}$  open-state 1:1 CaM:TRPV6 complex (Figs 2C,D). In  
36 order to identify the key TRPV6 residues essential for the formation of this complex,  
37 we employed alanine scanning mutagenesis and assessed the ability of each TRPV6  
38 mutant to bind to  $\text{CaM}_{\text{WT}}$ . This analysis identified three distinct parts to the TRPV6  
39 CaM binding interface, with the region S691-L703 functioning as the primary region  
40 for the CaM C-lobe interaction (Fig. 3C) and by analogy the residues involved in the  
41  $\text{CaM}_{12}$  interaction. This region is highly conserved between TRPV6<sup>691-703</sup>  
42 (SSANWERLRQGTL) and the equivalent part from TRPV5<sup>698-710</sup>  
43 (SHRGWEILRQNTL), with the latter extensively tested using electrophysiology  
44 experiments. Mutagenesis of the TRPV5 residues only increased  $\text{Ca}^{2+}$  uptake in  
45 HEK293 cells, most likely due to a reduced ability to bind  $\text{CaM}^{23}$ . Significantly, none  
46 of the mutations tested resulted in a reduced  $\text{Ca}^{2+}$  uptake i.e. suggestive of channel  
47 inactivation. Furthermore, the critical CaM N-lobe interacting TRPV6 region  
48  
49  
50  
51  
52  
53  
54  
55  
56  
57  
58

1  
2  
3 (704RRDLR<sup>708</sup>) identified in this study is not conserved within TRPV5  
4 (710GHLNL<sup>714</sup>). The full-length TRPV6 L707A mutant channel showed a  
5 significantly faster inactivation in our electrophysiology experiments (Figs 5D-J),  
6 which cannot be rationalised by a loss of the CaM:TRPV6 interaction. Finally, this  
7 effect constitutes the first observation of a mutation in a TRPV channel that results in  
8 faster inactivation; thus far all other mutations were only shown to abrogate the  
9 inactivation process.  
10  
11  
12  
13

14 In the X-ray structure of CaM and the related TRPV1 C-tail<sup>38</sup> TRPV1 residues  
15 784-798 are tightly embedded in a classical antiparallel 'closed' CaM conformation,  
16 simultaneously contacting both N- and C-lobes in a so-called 1-10 interaction motif  
17 (Fig. 3A). Our data indicate that the 1:1 CaM:TRPV6 complex is different, with  
18 separate regions of TRPV6 contacting either the N-lobe or the C-lobe exclusively  
19 (Figs 3C,D). Given the high degree of similarities of the C-lobe CSP patterns of the  
20 CaM<sub>12</sub> and CaM<sub>WT</sub> complexes for both TRPV6 (Figs 1D and 2C) and TRPV5<sup>52</sup>, the  
21 conformation of the C-lobe in complex with the channel tail is expect to be very  
22 similar in all cases. The complex of CaM<sub>12</sub> with the TRPV6 paralogue TRPV5  
23 displays a 1-5-8 CaM interaction motif, with a fully disengaged N-lobe<sup>52</sup> allowing for  
24 full adaptability of its orientation. We searched the PDB repository for structures of  
25 CaM<sub>WT</sub>:target complexes that could present a more suitable model for the fully Ca<sup>2+</sup>-  
26 loaded 1:1 CaM<sub>WT</sub>:TRPV6 complex. Three 1:1 CaM<sub>WT</sub>:peptide complexes, i.e.  
27 Munc13-1:CaM<sup>43</sup>,  $\alpha$ II-spectrin:CaM<sup>44</sup> and Matrix domain of HIV-1 gag:CaM<sup>45</sup>, were  
28 identified that each have a conserved tryptophan residue bound to the CaM C-lobe,  
29 similarly to TRPV6 and TRPV5, with a second hydrophobic residue bound to the  
30 CaM N-lobe, again similar to TRPV6. The peptides bind antiparallel to the CaM N-  
31 and C-lobes and the CaM N- and C-lobes display a much more open conformation.  
32 Interestingly, the larger the number of residues between the C-lobe bound tryptophan  
33 and the N-lobe bound hydrophobic residue, the more open the complex becomes. By  
34 sequence analogy alone, the CaM<sub>WT</sub>:TRPV6 complex would be expected to resemble  
35 the  $\alpha$ II-spectrin:CaM complex (PDB code 2FOT), while simultaneously suggesting  
36 that the peptide used in the X-ray studies of the CaM: TRPV1 complex may have  
37 been too short at the C-terminus to fully capture the analogous effects as reported in  
38 this study for TRPV6.  
39  
40  
41  
42  
43  
44  
45  
46  
47  
48  
49  
50  
51  
52  
53  
54  
55  
56  
57  
58  
59  
60

1  
2  
3 Until now, the full molecular mechanism(s) of TRP channel inactivation by  
4 CaM have been elusive. The most popular hypothesis, formulated for the TRPV1 and  
5 TRPV4 channels, proposes the formation of a ternary complex such that CaM bridges  
6 the channels N- and C-termini via N-tail-CaM N-lobe and CaM C-lobe C-tail  
7 complexes. Potentially, the formation of such a ternary complex could involve the  
8 distinct CaM N-lobe mediated second interaction surface we observed in the 1:2  
9 CaM:TRPV6 complex. However, within the TRPV subfamily CaM<sub>WT</sub> has only been  
10 shown to bind to the N-terminal cytosolic domain of TRPV1, TRPV3 and TRPV4 and  
11 not to TRPV2, TRPV5 or TRPV6<sup>46</sup>, rendering this mode of interaction for channel  
12 inactivation of the latter and potentially the whole TRPV sub-family, unlikely.  
13 Moreover, attempts to form such a complex for TRPV1 have so far proven  
14 unsuccessful<sup>38</sup>. In contrast, our two-tail hypothesis is backed by experimental data  
15 that include the formation of a specific 1:2 CaM:TRPV6 complex (Fig. 4) and fully  
16 explains the effects of the L707A mutation (Fig. 5) whereas the N-tail/C-tail CaM  
17 bridging model fails to explain the resulting experimentally observed effects.

18  
19 Our two-tail model hinges on the charging of the CaM N-lobe as the crucial  
20 Ca<sup>2+</sup>-sensing step with the C-tails not fully charged with CaM under basal Ca<sup>2+</sup>  
21 conditions, i.e. dependent on the local availability of the partially Ca<sup>2+</sup> loaded CaM.  
22 Once fully charged with Ca<sup>2+</sup>, the C-terminal region of the TRPV6 C-tail CaM  
23 binding site engages with the newly created hydrophobic pocket on the N-lobe via its  
24 L707 residue. Concomitantly, our model postulates that W695 from a second TRPV6  
25 C-tail competes and displaces L707 from the hydrophobic pocket, thus using CaM  
26 to form a bridge between two TRPV6 C-tails resulting in channel inactivation (Fig. 6).  
27 This mode of binding has also been observed in the structures of CaM with petunia  
28 glutamate decarboxylase, where two C-tail peptides interact simultaneously; each via  
29 a single tryptophan residue with either the CaM N- or C-lobes to form a 1:2  
30 CaM:peptide complex<sup>47,48</sup>. In addition, a similar structure was also determined for  
31 CaM interacting with the CaM binding domain of the tetrameric Orai1 channel, where  
32 a 1:2 CaM:channel complex was shown to occur *in vitro*<sup>49</sup>. Finally a pseudo-atomic  
33 structure of full-length tetrameric aquaporin-0 in complex with CaM<sup>50</sup> infers a  
34 mechanism of CaM mediated channel inactivation similar to the one proposed here  
35 for TRPV6.

36  
37 In conclusion, our data underpins a novel “two-tail” model for the CaM-  
38 mediated inactivation of the TRPV6 channel. This model comprises three  
39  
40  
41  
42  
43  
44  
45  
46  
47  
48  
49  
50  
51  
52  
53  
54  
55  
56  
57  
58  
59  
60

1  
2  
3 dynamically connected states in which differential interactions between the C-tails  
4 within the tetrameric channel and the CaM N- and C-lobes form the defining  
5 elements. Using a structure and interaction driven approach, we have characterised  
6 the crucial molecular components for each stage. Notably, we have identified the  
7 CaM N-lobe-mediated 1:2 CaM:TRPV6 complex formation as the key event that  
8 leads to channel inactivation. We have shown that the L707A mutation resulted in a  
9 significant increase in the rate of channel inactivation; an effect never previously  
10 observed within the TRPV family and that can only be explained by our “two-tail”  
11 model of CaM mediated TRPV channel inactivation.  
12  
13  
14  
15  
16  
17  
18  
19

### 20 **Acknowledgements**

21 We thank Dr. Fred Muskett for expert support and maintenance of our NMR  
22 equipment. GWV acknowledges funding during various stages of this project by  
23 BBSRC (grant BB/J007897/1) and MRC (grants MR/L000555/1 and  
24 MR/P00038X/1).  
25  
26  
27  
28  
29

### 30 **Supplementary materials**

31 Four Figures: evaluation of the integrity of all the CaM mutants, assessment of  
32 CaM<sub>1234</sub>, CaM<sub>123</sub>, CaM<sub>124</sub> and CaM<sub>34</sub> binding to the TRPV<sup>655-722</sup> fragment, and the  
33 full NMR analysis of all fifteen TRPV<sup>655-722</sup> mutants.  
34  
35  
36  
37  
38  
39  
40  
41  
42  
43  
44  
45  
46  
47  
48  
49  
50  
51  
52  
53  
54  
55  
56  
57  
58  
59  
60

## References

- (1) Montell, C. (2005) The TRP Superfamily of Cation Channels. *Science Signaling* 2005, re3–re3.
- (2) Nilius, B., and Owsianik, G. (2010) Transient receptor potential channelopathies. *Pflugers Arch.* 460, 437–450.
- (3) Chen, J., Luan, Y., Yu, R., Zhang, Z., Zhang, J., and Wang, W. (2014) Transient receptor potential (TRP) channels, promising potential diagnostic and therapeutic tools for cancer. *BST* 8, 1–10.
- (4) Liao, M., Cao, E., Julius, D., and Cheng, Y. (2013) Structure of the TRPV1 ion channel determined by electron cryo-microscopy. *Nature* 504, 107–112.
- (5) Zubcevic, L., Herzik, M. A., Chung, B. C., Liu, Z., Lander, G. C., and Lee, S.-Y. (2016) Cryo-electron microscopy structure of the TRPV2 ion channel. *Nat Struct Mol Biol* 23, 180–186.
- (6) Hughes, T. E. T., Lodowski, D. T., Huynh, K. W., Yazici, A., Del Rosario, J., Kapoor, A., Basak, S., Samanta, A., Han, X., Chakrapani, S., Zhou, Z. H., Filizola, M., Rohacs, T., Han, S., and Moiseenkova-Bell, V. Y. (2018) Structural basis of TRPV5 channel inhibition by econazole revealed by cryo-EM. *Nat Struct Mol Biol* 1–12.
- (7) Paulsen, C. E., Armache, J.-P., Gao, Y., Cheng, Y., and Julius, D. (2015) Structure of the TRPA1 ion channel suggests regulatory mechanisms. *Nature* 520, 511–517.
- (8) Saotome, K., Singh, A. K., Yelshanskaya, M. V., and Sobolevsky, A. I. (2016) Crystal structure of the epithelial calcium channel TRPV6. *Nature* 534, 506–511.
- (9) McGoldrick, L. L., Singh, A. K., Saotome, K., Yelshanskaya, M. V., Twomey, E. C., Grassucci, R. A., and Sobolevsky, A. I. (2018) Opening of the human epithelial calcium channel TRPV6. *Nature* 553, 233–237.
- (10) Li, M., Yu, Y., and Yang, J. (2010) Structural Biology of TRP Channels, in *Advances in Experimental Medicine and Biology*, pp 1–23. Springer Netherlands, Dordrecht.
- (11) Hoenderop, J. G. J. (2005) Calcium Absorption Across Epithelia. *Physiological Reviews* 85, 373–422.
- (12) Peng, J.-B., Chen, X.-Z., Berger, U. V., Weremowicz, S., Morton, C. C., Vassilev, P. M., Brown, E. M., and Hediger, M. A. (2000) Human Calcium Transport Protein CaT1. *Biochem. Biophys. Res. Commun.* 278, 326–332.

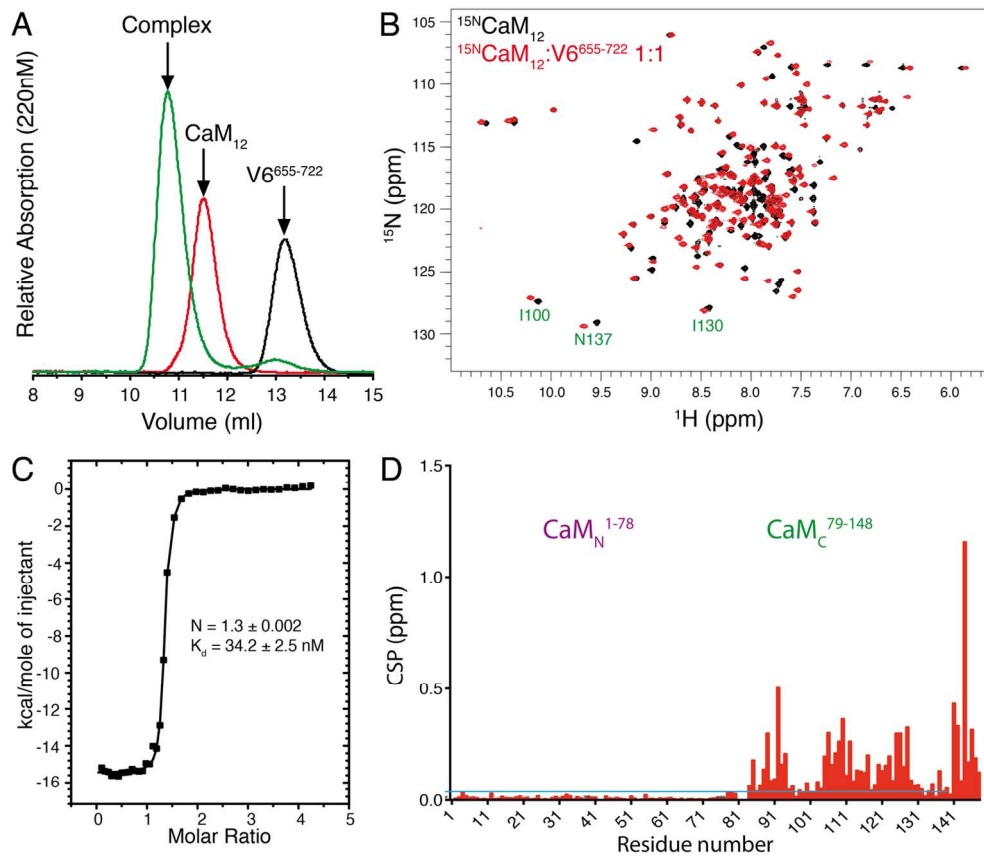
- 1  
2  
3 (13) Vennekens, R., Hoenderop, J., Prenen, J., Stuiver, M., Willems, P., Droogmans,  
4 G., Nilius, B., and Bindels, R. (2000) Permeation and gating properties of the  
5 novel epithelial Ca<sup>2+</sup> channel. *J. Biol. Chem.* 275, 3963–3969.  
6  
7  
8 (14) Hoenderop, J., van der Kemp, A., Hartog, A., van de Graaf, S., van Os, C. H.,  
9 Willems, P., and Bindels, R. (1999) Molecular identification of the apical Ca<sup>2+</sup>  
10 channel in 1,25-dihydroxyvitamin D-3-responsive epithelia. *J. Biol. Chem.* 274,  
11 8375–8378.  
12  
13  
14 (15) Hoenderop, J. G. J., van Leeuwen, J. P. T. M., van der Eerden, B. C. J., Kersten,  
15 F. F. J., van der Kemp, A. W. C. M., Mérillat, A.-M., Waarsing, J. H., Rossier, B.  
16 C., Vallon, V., Hummler, E., and Bindels, R. J. M. (2003) Renal Ca<sup>2+</sup> wasting,  
17 hyperabsorption, and reduced bone thickness in mice lacking TRPV5. *J. Clin.*  
18 *Invest.* 112, 1906–1914.  
19  
20  
21  
22 (16) Weissgerber, P., Kriebs, U., Tsvilovskyy, V., Olausson, J., Kretz, O., Stoerger,  
23 C., Mannebach, S., Wissenbach, U., Vennekens, R., Middendorff, R., Flockerzi,  
24 V., and Freichel, M. (2012) Excision of Trpv6 Gene Leads to Severe Defects in  
25 Epididymal Ca<sup>2+</sup> Absorption and Male Fertility Much Like Single D541A Pore  
26 Mutation. *Journal of Biological Chemistry* 287, 17930–17941.  
27  
28  
29  
30 (17) Derler, I., Hofbauer, M., Kahr, H., Fritsch, R., Muik, M., Kepplinger, K., Hack,  
31 M. E., Moritz, S., Schindl, R., Groschner, K., and Romanin, C. (2006) Dynamic  
32 but not constitutive association of calmodulin with rat TRPV6 channels enables  
33 fine tuning of Ca<sup>2+</sup>-dependent inactivation. *The Journal of Physiology* 577, 31–  
34 44.  
35  
36  
37  
38 (18) Cao, C., Zakharian, E., Borbiri, I., and Rohacs, T. (2013) Interplay between  
39 Calmodulin and Phosphatidylinositol 4,5-Bisphosphate in Ca<sup>2+</sup>-induced  
40 Inactivation of Transient Receptor Potential Vanilloid 6 Channels. *Journal of*  
41 *Biological Chemistry* 288, 5278–5290.  
42  
43  
44  
45 (19) Lambers, T. T., Mahieu, F., Oancea, E., Hoofd, L., de Lange, F., Mensenkamp,  
46 A. R., Voets, T., Nilius, B., Clapham, D. E., Hoenderop, J. G., and Bindels, R. J.  
47 (2006) Calbindin-D-28K dynamically controls TRPV5-mediated Ca<sup>2+</sup> transport.  
48 *Embo Journal* 25, 2978–2988.  
49  
50  
51 (20) Gkika, D., Mahieu, F., Nilius, B., Hoenderop, J. G. J., and Bindels, R. J. M.  
52 (2004) 80K-H as a New Ca<sup>2+</sup> Sensor Regulating the Activity of the Epithelial  
53 Ca<sup>2+</sup> Channel Transient Receptor Potential Cation Channel V5 (TRPV5).  
54 *Journal of Biological Chemistry* 279, 26351–26357.  
55  
56  
57  
58  
59  
60

- 1  
2  
3 (21) Niemeyer, B. A., Bergs, C., Wissenbach, U., Flockerzi, V., and Trost, C. (2001)  
4 Competitive regulation of CaT-like-mediated Ca<sup>2+</sup> entry by protein kinase C and  
5 calmodulin. *Proc. Natl. Acad. Sci. U.S.A.* 98, 3600–3605.  
6  
7 (22) Lambers, T. T., Weidema, A. F., Nilius, B., Hoenderop, J. G. J., and Bindels, R.  
8 J. M. (2004) Regulation of the Mouse Epithelial Ca<sup>2+</sup> Channel TRPV6 by the  
9 Ca<sup>2+</sup>-sensor Calmodulin. *Journal of Biological Chemistry* 279, 28855–28861.  
10  
11 (23) de Groot, T., Kovalevskaya, N. V., Verkaart, S., Schilderink, N., Felici, M., van  
12 der Hagen, E. A. E., Bindels, R. J. M., Vuister, G. W., and Hoenderop, J. G.  
13 (2011) Molecular Mechanisms of Calmodulin Action on TRPV5 and Modulation  
14 by Parathyroid Hormone. *Molecular and Cellular Biology* 31, 2845–2853.  
15  
16 (24) Kovalevskaya, N. V., Bokhovchuk, F. M., and Vuister, G. W. (2012) The  
17 TRPV5/6 calcium channels contain multiple calmodulin binding sites with  
18 differential binding properties. *J Struct Funct Genomics* 13, 91–100.  
19  
20 (25) Kovalevskaya, N. V., Schilderink, N., and Vuister, G. W. (2011) Expression and  
21 purification of the C-terminal fragments of TRPV5/6 channels. *Protein*  
22 *Expression and Purification* 80, 28-33.  
23  
24 (26) Nilius, B., Weidema, F., Prenen, J., Hoenderop, J. G., Vennekens, R., Hoefs, S.,  
25 Droogmans, G., and Bindels, R. J. (2003) The carboxyl terminus of the epithelial  
26 Ca<sup>2+</sup> channel ECaC1 is involved in Ca<sup>2+</sup>-dependent inactivation. *Pflugers Arch.*  
27 445, 584–588.  
28  
29 (27) Singh, B. B., Liu, X. B., Tang, J. S., Zhu, M. X., and Ambudkar, I. S. (2002)  
30 Calmodulin regulates Ca<sup>2+</sup>-dependent feedback inhibition of store-operated  
31 interaction with a site in the Ca<sup>2+</sup> influx by C terminus of TrpC1. *Molecular Cell*  
32 9, 739–750.  
33  
34 (28) Numazaki, M., Tominaga, T., Takeuchi, K., Murayama, N., Toyooka, H., and  
35 Tominaga, M. (2003) Structural determinant of TRPV1 desensitization interacts  
36 with calmodulin. *Proc. Natl. Acad. Sci. U.S.A.* 100, 8002–8006.  
37  
38 (29) Strotmann, R., Schultz, G., and Plant, T. D. (2003) Ca<sup>2+</sup>-dependent Potentiation  
39 of the Nonselective Cation Channel TRPV4 Is Mediated by a C-terminal  
40 Calmodulin Binding Site. *Journal of Biological Chemistry* 278, 26541–26549.  
41  
42 (30) Mercado, J., Gordon-Shaag, A., Zagotta, W. N., and Gordon, S. E. (2010) Ca<sup>2+</sup>-  
43 Dependent Desensitization of TRPV2 Channels Is Mediated by Hydrolysis of  
44 Phosphatidylinositol 4,5-Bisphosphate. *Journal of Neuroscience* 30, 13338–  
45 13347.  
46  
47  
48  
49  
50  
51  
52  
53  
54  
55  
56  
57  
58  
59  
60

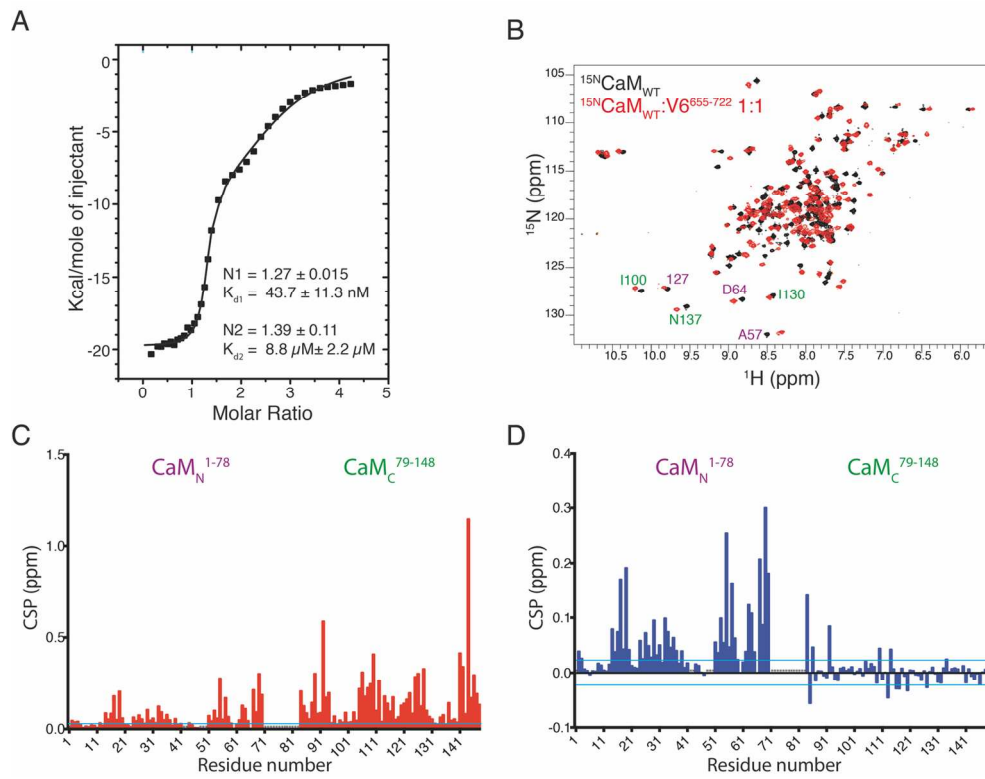
- 1  
2  
3 (31) Kovalevskaya, N. V., van de Waterbeemd, M., Bokhovchuk, F. M., Bate, N.,  
4 Bindels, R. J. M., Hoenderop, J. G. J., and Vuister, G. W. (2013) Structural  
5 analysis of calmodulin binding to ion channels demonstrates the role of its  
6 plasticity in regulation. *Pflugers Arch.* 465, 1507–1519.  
7  
8 (32) Tidow, H., and Nissen, P. (2013) Structural diversity of calmodulin binding to its  
9 target sites. *FEBS J.* 280, 5551–5565.  
10  
11 (33) Linse, S., Helmersson, A., And Forsen, S. (1991) Calcium-Binding to  
12 Calmodulin and Its Globular Domains. *J. Biol. Chem.* 266, 8050–8054.  
13  
14 (34) Bate, N., Gingras, A. R., Bachir, A., Horwitz, R., Ye, F., Patel, B., Goult, B. T.,  
15 and Critchley, D. R. (2012) Talin contains a C-terminal calpain2 cleavage site  
16 important in focal adhesion dynamics. *PLoS ONE* 7, e34461.  
17  
18 (35) Williamson, R. A., Carr, M. D., Frenkiel, T. A., Feeney, J., and Freedman, R. B.  
19 (1997) Mapping the binding site for matrix metalloproteinase on the N-terminal  
20 domain of the tissue inhibitor of metalloproteinases-2 by NMR chemical shift  
21 perturbation. *Biochemistry* 36, 13882–13889.  
22  
23 (36) Wu, P.-R., Kuo, C.-C., Yet, S.-F., Liou, J.-Y., Wu, K. K., and Chen, P.-F. (2012)  
24 Lobe-Specific Calcium Binding in Calmodulin Regulates Endothelial Nitric  
25 Oxide Synthase Activation. *PLoS ONE* (Hofmann, A., Ed.) 7, e39851.  
26  
27 (37) Babu, Y. S., Bugg, C. E., and Cook, W. J. (1988) Structure of calmodulin refined  
28 at 2.2 Å resolution. *J. Mol. Biol.* 204, 191–204.  
29  
30 (38) Lau, S. Y., Procko, E., and Gaudet, R. (2012) Distinct properties of Ca<sup>2+</sup>-  
31 calmodulin binding to N- and C-terminal regulatory regions of the TRPV1  
32 channel. *The Journal of General Physiology* 140, 541–555.  
33  
34 (39) Muskett, F. W., Frenkiel, T. A., Feeney, J., Freedman, R. B., Carr, M. D., and  
35 Williamson, R. A. (1998) High resolution structure of the N-terminal domain of  
36 tissue inhibitor of metalloproteinases-2 and characterization of its interaction site  
37 with matrix metalloproteinase-3. *J. Biol. Chem.* 273, 21736–21743.  
38  
39 (40) Nilius, B., Prenen, J., Hoenderop, J. G. J., Vennekens, R., Hoefs, S., Weidema,  
40 A. F., Droogmans, G., and Bindels, R. J. M. (2002) Fast and Slow Inactivation  
41 Kinetics of the Ca<sup>2+</sup> Channels ECaC1 and ECaC2 (TRPV5 and TRPV6). Role  
42 Of The Intracellular Loop Located Between Transmembrane Segments 2 And 3.  
43 *Journal of Biological Chemistry* 277, 30852–30858.  
44  
45 (41) Persechini, A., and Cronk, B. (1999) The relationship between the free  
46 concentrations of Ca<sup>2+</sup> and Ca<sup>2+</sup>-calmodulin in intact cells. *J. Biol. Chem.* 274,  
47  
48  
49  
50  
51  
52  
53  
54  
55  
56  
57  
58  
59

- 6827–6830.
- (42) Erickson, M. G., Alseikhan, B. A., Peterson, B. Z., and Yue, D. T. (2001) Preassociation of calmodulin with voltage-gated Ca<sup>2+</sup> channels revealed by FRET in single living cells. *Neuron* 31, 973–985.
- (43) Rodríguez-Castañeda, F., Maestre-Martínez, M., Coudeville, N., Dimova, K., Junge, H., Lipstein, N., Lee, D., Becker, S., Brose, N., Jahn, O., Carlomagno, T., and Griesinger, C. (2010) Modular architecture of Munc13/calmodulin complexes: dual regulation by Ca<sup>2+</sup> and possible function in short-term synaptic plasticity. *Embo Journal* 29, 680–691.
- (44) Simonovic, M., Zhang, Z., Cianci, C. D., Steitz, T. A., and Morrow, J. S. (2006) Structure of the calmodulin alpha II-spectrin complex provides insight into the regulation of cell plasticity. *J. Biol. Chem.* 281, 34333–34340.
- (45) Vlach, J., Samal, A. B., and Saad, J. S. (2014) Solution Structure of Calmodulin Bound to the Binding Domain of the HIV-1 Matrix Protein. *J. Biol. Chem.* 289, 8697–8705.
- (46) Phelps, C. B., Wang, R. R., Choo, S. S., and Gaudet, R. (2009) Differential Regulation of TRPV1, TRPV3, and TRPV4 Sensitivity through a Conserved Binding Site on the Ankyrin Repeat Domain. *Journal of Biological Chemistry* 285, 731–740.
- (47) Yuan, T., and Vogel, H. J. (1998) Calcium-Calmodulin-induced Dimerization of the Carboxyl-terminal Domain from Petunia Glutamate Decarboxylase: A Novel Calmodulin-Peptide Interaction Motif. *Journal of Biological Chemistry* 273, 30328–30335.
- (48) Yap, K. L., Yuan, T., Mal, T. K., Vogel, H. J., and Ikura, M. (2003) Structural Basis for Simultaneous Binding of Two Carboxy-terminal Peptides of Plant Glutamate Decarboxylase to Calmodulin. *J. Mol. Biol.* 328, 193–204.
- (49) Liu, Y., Zheng, X., Mueller, G. A., Sobhany, M., DeRose, E. F., Zhang, Y., London, R. E., and Birnbaumer, L. (2012) Crystal Structure of Calmodulin Binding Domain of Orai1 in Complex with Ca<sup>2+</sup>\*Calmodulin Displays a Unique Binding Mode. *Journal of Biological Chemistry* 287, 43030–43041.
- (50) Reichow, S. L., Clemens, D. M., Freitas, J. A., Németh-Cahalan, K. L., Heyden, M., Tobias, D. J., Hall, J. E., and Gonen, T. (2013) Allosteric mechanism of water-channel gating by Ca<sup>2+</sup>–calmodulin. *Nat Struct Mol Biol* 20, 1085–1092.

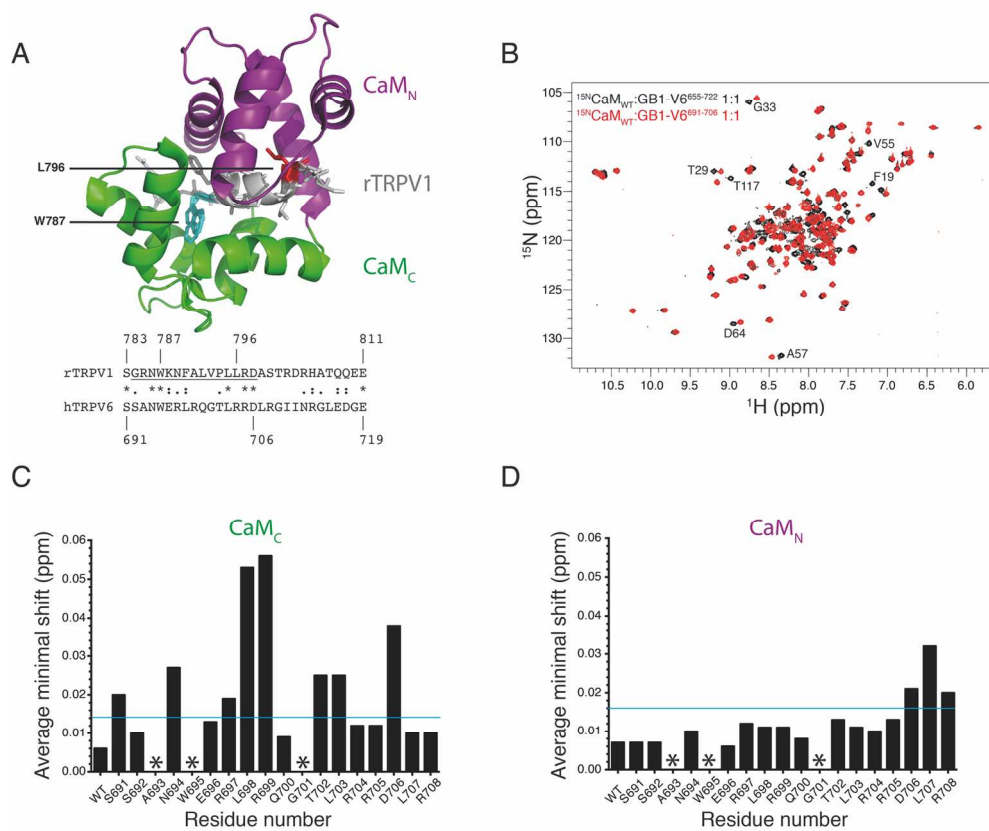
- 1  
2  
3 (51) Skinner, S.P., Fogh, R.H., Boucher, W., Ragan, T.J., Mureddu, L. and Vuister,  
4 G.W. (2016). CcpNmr AnalysisAssign: a flexible platform for integrated NMR  
5 analysis. *Journal of Biomolecular NMR* 66, 111–124.  
6  
7  
8 (52) Bokhovchuk, F.M., Bate, N., Kovalevskaya, N. Goult, B.T., Spronk, C.A.E.M.,  
9 and Vuister, G.W. , (2018) *Biochemistry*, THIS ISSUE.  
10  
11  
12  
13  
14  
15  
16  
17  
18  
19  
20  
21  
22  
23  
24  
25  
26  
27  
28  
29  
30  
31  
32  
33  
34  
35  
36  
37  
38  
39  
40  
41  
42  
43  
44  
45  
46  
47  
48  
49  
50  
51  
52  
53  
54  
55  
56  
57  
58  
59  
60



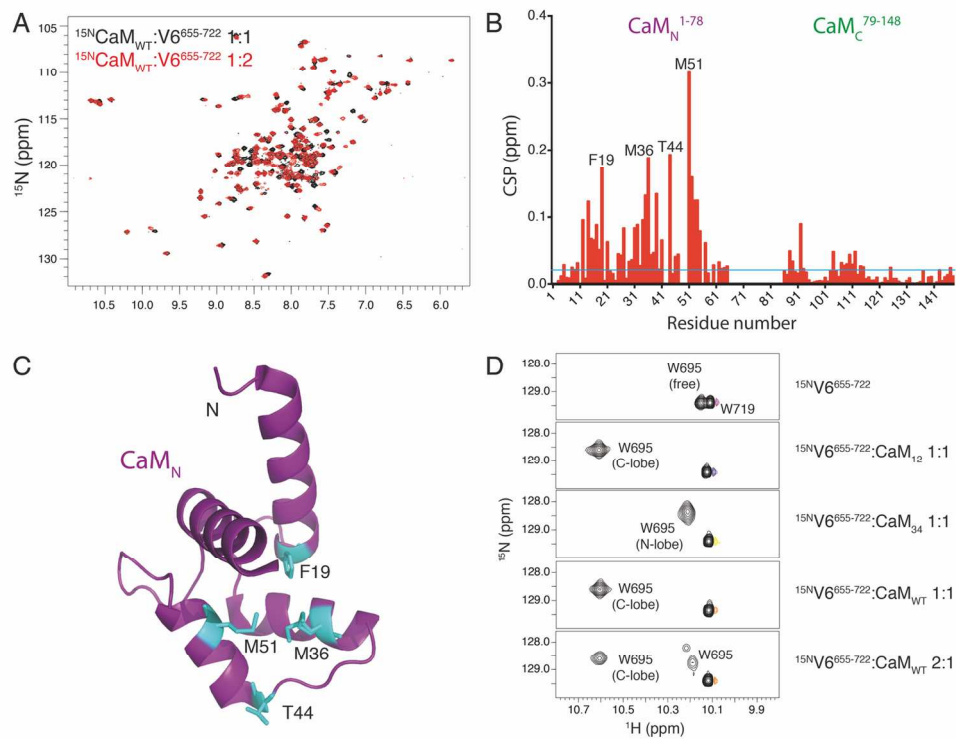
139x126mm (300 x 300 DPI)



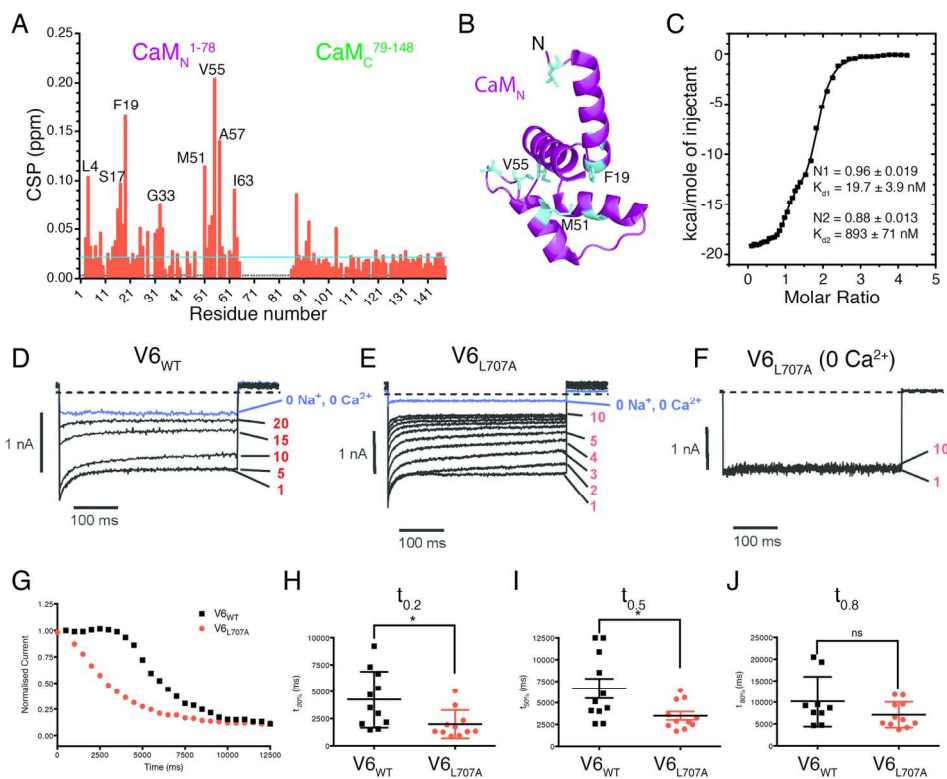
139x107mm (300 x 300 DPI)



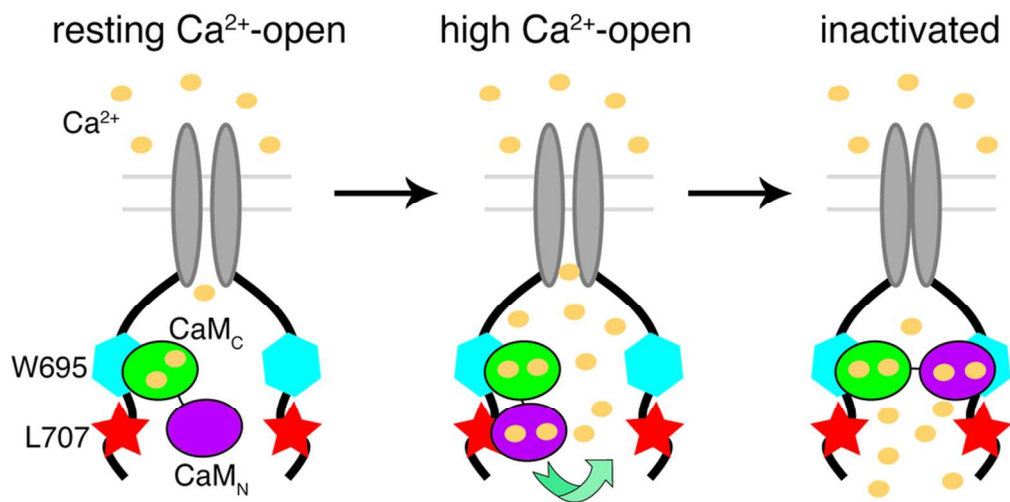
147x124mm (300 x 300 DPI)



144x112mm (300 x 300 DPI)

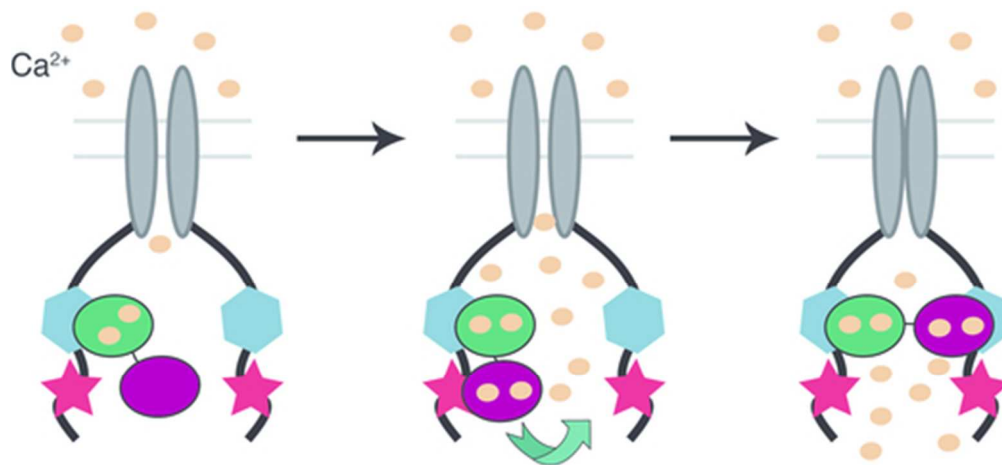


145x112mm (300 x 300 DPI)



86x44mm (300 x 300 DPI)

TOC: "For Table of Contents use only"



TOC "For Table of Contents use only"

44x24mm (300 x 300 DPI)

